The Astrophysical Journal, 601:319–339, 2004 January 20

AN EXTENDED STAR FORMATION HISTORY FOR THE GALACTIC CENTER FROM *HUBBLE SPACE TELESCOPE* NICMOS OBSERVATIONS[1]

Donald F. Figer,[2,3] R. Michael Rich,[4] Sungsoo S. Kim,[5] Mark Morris,[4] and Eugene Serabyn[6]
Received 2003 July 19; accepted 2003 September 18

ABSTRACT

We present *Hubble Space Telescope* (*HST*) Near-Infrared Camera and Multiobject Spectrometer (NICMOS) observations as evidence that continuous star formation has created much of the central stellar cusp of the Galaxy. The data are the deepest ever obtained for a Galactic center population, being more than 50% complete for $m_{\rm F205W} < 19.3$, or initial stellar masses $\gtrsim 2\ M_\odot$. We use Geneva and Padova stellar evolution models to produce synthetic luminosity functions for burst and continuous star formation scenarios, finding that the observations are fitted best by continuous star formation at a rate that is consistent with the recent star formation activity that produced the three massive young clusters in the central 50 pc. Further, it is not possible to fit the observations with ancient burst models, such as would be appropriate for an old population like that in Baade's window or NGC 6528.

Subject headings: Galaxy: bulge — Galaxy: center — infrared: stars — stars: formation

1. INTRODUCTION

The Milky Way Galaxy is composed of several distinct stellar components, including the disk, the bulge, and the halo. In addition to these well-known populations, new evidence suggests that there is yet another stellar population in the central part of the bulge, composed of both young and old stars. The old component has often been associated with the inward extension of the ancient bulge, and the young stars are generally clustered in the central parsec and in two massive clusters about 30 pc to the north of the center. Stars in the central region are currently forming in several molecular clouds, e.g., Sgr B2. On scales covering a few hundred parsecs, Serabyn & Morris (1996) identify a peak in the infrared surface brightness distribution, scaling as $1/r$ in *COBE* data, associating this feature with light from a massive cluster of stars having a $1/r^2$ volume density distribution, the "r^{-2} cusp" (Hiromoto et al. 1984). Serabyn & Morris (1996) suggest that the cusp is composed of stars created continuously over the lifetime of the Galaxy. Launhardt, Zylka, & Mezger (2002) find a central disk in the *COBE* imagery of the Galactic center (GC) and identify this component with the central cusp.

Catchpole, Whitelock, & Glass (1990) resolve this cusp (over degree scales) into individual bright stars and argue that the overall stellar population was likely to be of intermediate age, with the youngest population more concentrated toward the center. Others find similar evidence in support of an intermediate-age stellar population in the GC (mostly in the central few arcminutes), e.g., Rieke (1987, 1993), Haller (1992), Haller & Rieke (1989), Lebofsky & Rieke (1987), Blum, DePoy, & Sellgren (1995), Narayanan, Gould, & DePoy (1996), and Sjouwerman et al. (1999). Frogel, Tiede, & Kuchinski (1999) present some of the strongest evidence associating the r^{-2} cusp with an intermediate population, finding that the density of young stars near the GC declines much more rapidly with Galactocentric radius than does the density of the ancient bulge population.

The evidence for very recent (<10 Myr) star formation in the GC abounds. The Lyman continuum flux emitted in the central few degrees of the Galaxy is $\sim 10^{52}$ photons s^{-1} (Cox & Laureijs 1989), half coming from stars in the three massive young clusters in the central 50 pc (Figer, McLean, & Morris 1999b; Figer et al. 2002). This represents about 10% of the total Lyman continuum flux for the whole Galaxy, and the number of massive stars ($M_{\rm init} > 20\ M_\odot$ in the context of this paper) in the clusters is also about 10% of the number in the whole Galaxy. However, the star formation rate in the GC is ~1% of the total star formation rate in the Galaxy, as judged by simply dividing the mass in known, recently formed stars by the duration of the star formation episodes that formed those stars, i.e., $5 \times 10^4\ M_\odot/5$ Myr $\sim 0.01\ M_\odot$ yr^{-1}, giving a star formation rate density of $10^{-7}\ M_\odot$ yr^{-1} pc^{-3}. This rate is roughly a factor of 250 higher than the mean rate in the Galaxy and about the same factor lower than the rate in starburst galaxies. Such a low star formation rate compared to Lyman continuum photon production necessarily follows from the relatively flat initial mass function slope estimated by Figer et al. (1999a) and used in estimating the mass of stars formed in the young clusters.

The young stellar clusters in the GC are extraordinary. The Central cluster is located within the central parsec and contains over 30 massive stars (Genzel et al. 1996). Only 30 pc distant, by projection, from the center are the Arches (Cotera et al. 1994, 1996; Figer 1995; Nagata et al. 1995; Cotera 1995; Serabyn, Shupe, & Figer 1998; Figer et al. 1999a, 2002) and Quintuplet clusters (Okuda et al. 1990; Nagata et al. 1990; Glass, Moneti, & Moorwood 1990; Moneti, Glass, & Moorwood 1992, 1994; Geballe et al. 1994; Figer, McLean, & Morris 1995; Figer et al.

[1] Based on observations with the NASA/ESA *Hubble Space Telescope*, obtained at the Space Telescope Science Institute, which is operated by the Association of Universities for Research in Astronomy (AURA), Inc., under NASA contract NAS5-26555.

[2] Space Telescope Science Institute, 3700 San Martin Drive, Baltimore, MD 21218; figer@stsci.edu.
[3] Department of Physics and Astronomy, Johns Hopkins University, Baltimore, MD 21218.
[4] Department of Physics and Astronomy, Division of Astronomy, UCLA, Los Angeles, CA 90095-1562.
[5] Department of Astronomy and Space Science, Kyung Hee University, Yongin-shi 449-701, Korea.
[6] California Institute of Technology, MS 320-47, Pasadena, CA 91125; eserabyn@huey.jpl.nasa.gov.

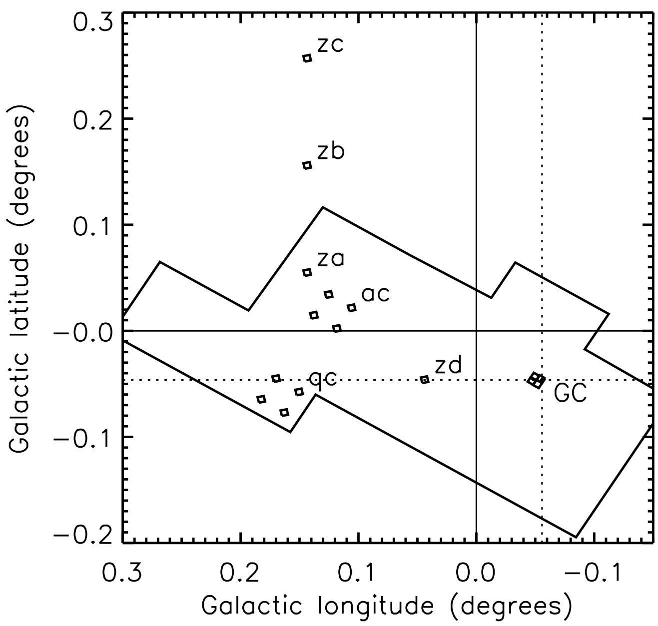

FIG. 1.—Fields covered by observations. Labels are overplotted for the NICMOS "z-fields" (za, zb, zc, and zd), the cluster control fields (ac and qc), and the Gemini AO fields (the four fields nearest the "GC" label). The Lick field is marked by the large, irregularly shaped box (Figer 1995). Coordinates for the fields are given in Table 1.

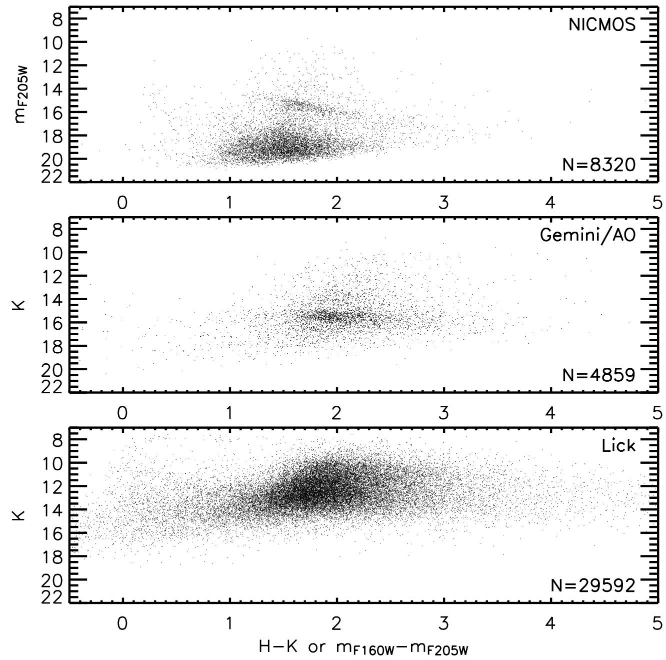

FIG. 2.—Observed CMDs for NICMOS (*top*), Gemini (*middle*), and Lick data (*bottom*). The red clump can be seen best in the NICMOS data, starting at $H-K \approx 1.5$ and $K \approx 15$, and continuing to the lower right; the extension toward the lower right is a result of differential reddening dispersing the stars along the reddening vector.

1999a, 1999b). The Arches cluster contains at least 150 O stars within a diameter of 0.6 pc, making this cluster the densest in the Galaxy (Figer et al. 1999a). A list of the 30 most massive stars in the Quintuplet cluster is given in Figer et al. (1999b). All three clusters are quite similar in most respects, except for age; the Central and Quintuplet clusters are ≈3–5 Myr old (Figer et al. 1999b; Krabbe et al. 1995; Najarro et al. 1997), while the Arches cluster is substantially younger, $\tau_{\rm age} = 2.5 \pm 0.5$ Myr (Figer et al. 2002). With such a collection of young, massive clusters, is it possible that we are witnessing an extraordinary burst of star formation in the GC, or has the center hosted similar bursts of star formation throughout its long history? Further, what is the fate of these massive clusters?

Kim, Morris, & Lee (1999), Kim et al. (2000), and Portegies Zwart et al. (2001) argue that the young clusters in the GC will be tidally disrupted in ≲10–50 Myr. This might explain the absence of older clusters of similar masses in this region.

TABLE 1
LOG OF OBSERVATIONS

Field	R.A. (B1950.0)	Decl. (B1950.0)	Longitude (deg)	ΔLongitude[a] (pc)	Latitude (deg)	ΔLatitude[a] (pc)	Instrument
Quintuplet.......	17 43 04.80	−28 48 26.0	0.1664	31.6	−0.0611	−1.5	*HST* NICMOS
Arches	17 42 39.90	−28 48 13.0	0.1218	25.4	0.0182	9.5	*HST* NICMOS
za	17 42 34.47	−28 45 57.1	0.1435	28.4	0.0549	14.6	*HST* NICMOS
zb	17 42 10.96	−28 42 45.9	0.1435	28.4	0.1559	28.7	*HST* NICMOS
zc	17 41 47.47	−28 39 34.4	0.1435	28.4	0.2569	42.9	*HST* NICMOS
zd	17 42 43.68	−28 54 13.2	0.0439	14.5	−0.0461	0.5	*HST* NICMOS
GC	17 42 30.00	−28 53 00.0	0.0350	12.7	0.0070	7.4	Lick/Gemini
Gemini 1	17 42 29.22	−28 59 19.4	−0.0548	0.13	−0.0455	0.11	Gemini AO/Hokupa'a+ Quirc
Gemini 2	17 42 29.37	−28 58 59.4	−0.0498	0.83	−0.0430	0.46	Gemini AO/Hokupa'a+ Quirc
Gemini 5	17 42 30.73	−28 59 19.5	−0.0519	0.53	−0.0502	−0.54	Gemini AO/Hokupa'a+ Quirc
Gemini 6	17 42 30.82	−28 58 59.5	−0.0470	1.22	−0.0476	−0.17	Gemini AO/Hokupa'a+ Quirc

NOTE.—Units of right ascension are hours, minutes, and seconds, and units of declination are degrees, arcminutes, and arcseconds.
[a] Values are with respect to GC, located at (−0°.0557, −0°.0463).

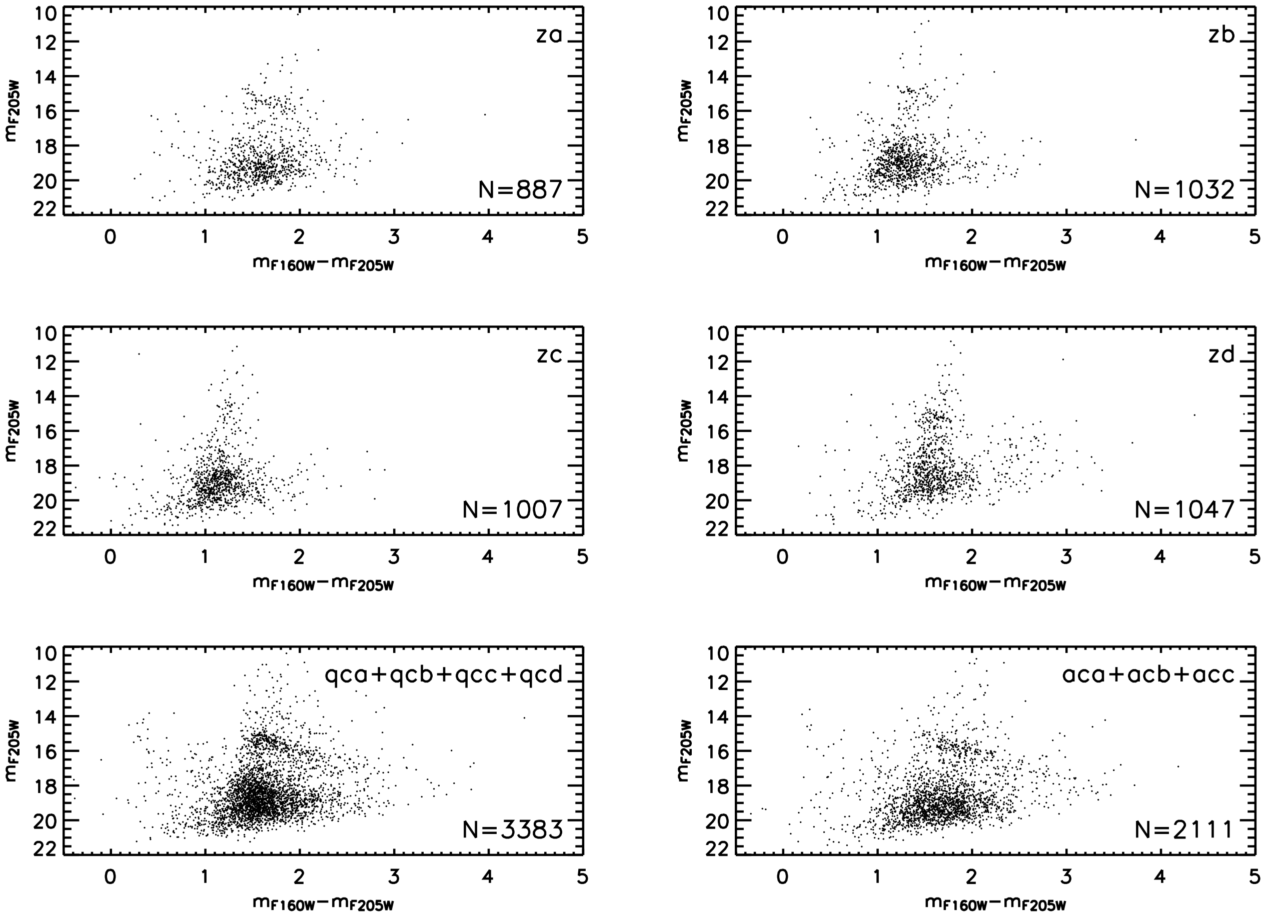

FIG. 3.—Observed CMDs for individual NICMOS fields. Indications of a red clump can be seen in all fields at locations that are dependent on the average extinction for each field. For example, the red clump has a color of $m_{\rm F160W}-m_{\rm F205W} \approx 1.5$ for the zd field, the field that is nearest to the GC and suffers the highest extinction of the six fields. The zc field is farthest from the GC and therefore has the lowest extinction and a red clump that is relatively blue compared to those in the other fields. Note that the gap between the main sequence ($m_{\rm F205W} \approx 19$) and the red clump ($m_{\rm F205W} \approx 15.5$) is more populated for fields nearer the GC, e.g., in the zd field, suggesting a trend of younger stars toward the center.

Gerhard (2001) argues that such clusters should spiral into the central parsec on relatively short timescales, i.e., that the He I stars in the central cluster might contain stellar products of a dense cluster formed well outside the central parsec. In this scenario, the stars are drawn inward to the central parsec by dynamical friction between the cluster and the tidal field of the GC. Kim, Morris, & Figer (2003) and Kim & Morris (2003) explore this possibility using *N*-body simulations, finding that dynamical friction is unlikely to have produced the population presently seen in the central parsec.

Clearly, the GC has formed a plethora of stars in the past 5 Myr, but it is less apparent when the bulk of stars in the central 50 pc formed. If we assume that the star formation rate in the past was similar to the present rate, then the total mass of stars formed over the past 10 Gyr is $\approx 10^8 \, M_\odot$ within a radius of 30 pc of the GC, or an order of magnitude greater than this amount over the whole central molecular zone (CMZ), as first suggested by Serabyn & Morris (1996).

This paper reports new, deep imaging of several fields in the central 100 pc of the Galaxy. Our imaging solidly reaches the helium-burning clump giant stars and just reaches the old main-sequence turnoff point. We model the luminosity functions (LFs) to explore the star formation history of the GC. We argue that the best fit to the total number of stars and to the LFs requires an approximately continuous star formation history over the last $\sim$10 Gyr.

2. OBSERVATIONS

The Galactic center observational data are taken from Figer (1995), Gemini AO (adaptive optics) science verification observations,[7] and NICMOS observations obtained as a part of *Hubble Space Telescope* (*HST*) program GO-7364. The field locations are shown in Figure 1 and listed in Table 1.

The Lick data cover 40 fields, in a mosaic, obtained at the Shane 3 m telescope at Lick Observatory in the H ($\lambda_{\rm cen} = 1.65\ \mu$m) and K' ($\lambda_{\rm cen} = 2.12\ \mu$m) filters. The individual images cover $3' \times 3'$ of area, while the mosaic spans $24' \times 14'$ of area, oriented with the long axis north-south and centered $6'$ to the north of the GC. The exposure times were 35 s for each image.

The Gemini AO data were obtained as part of the Gemini North commissioning observing run using the Hokupa'a+Quirc instrument in the H and K' bands. The field size is $20'' \times 20''$. These data cover four fields (1, 2, 5, and 6), arranged in a mosaic centered about $15''$ to the north and east of the GC. Both the

[7] Based on observations obtained at the Gemini Observatory, which is operated by the AURA, Inc., under a cooperative agreement with the NSF on behalf of the Gemini partnership: the National Science Foundation (United States), the Particle Physics and Astronomy Research Council (United Kingdom), the National Research Council (Canada), CONICYT (Chile), the Australian Research Council (Australia), CNPq (Brazil), and CONICET (Argentina).

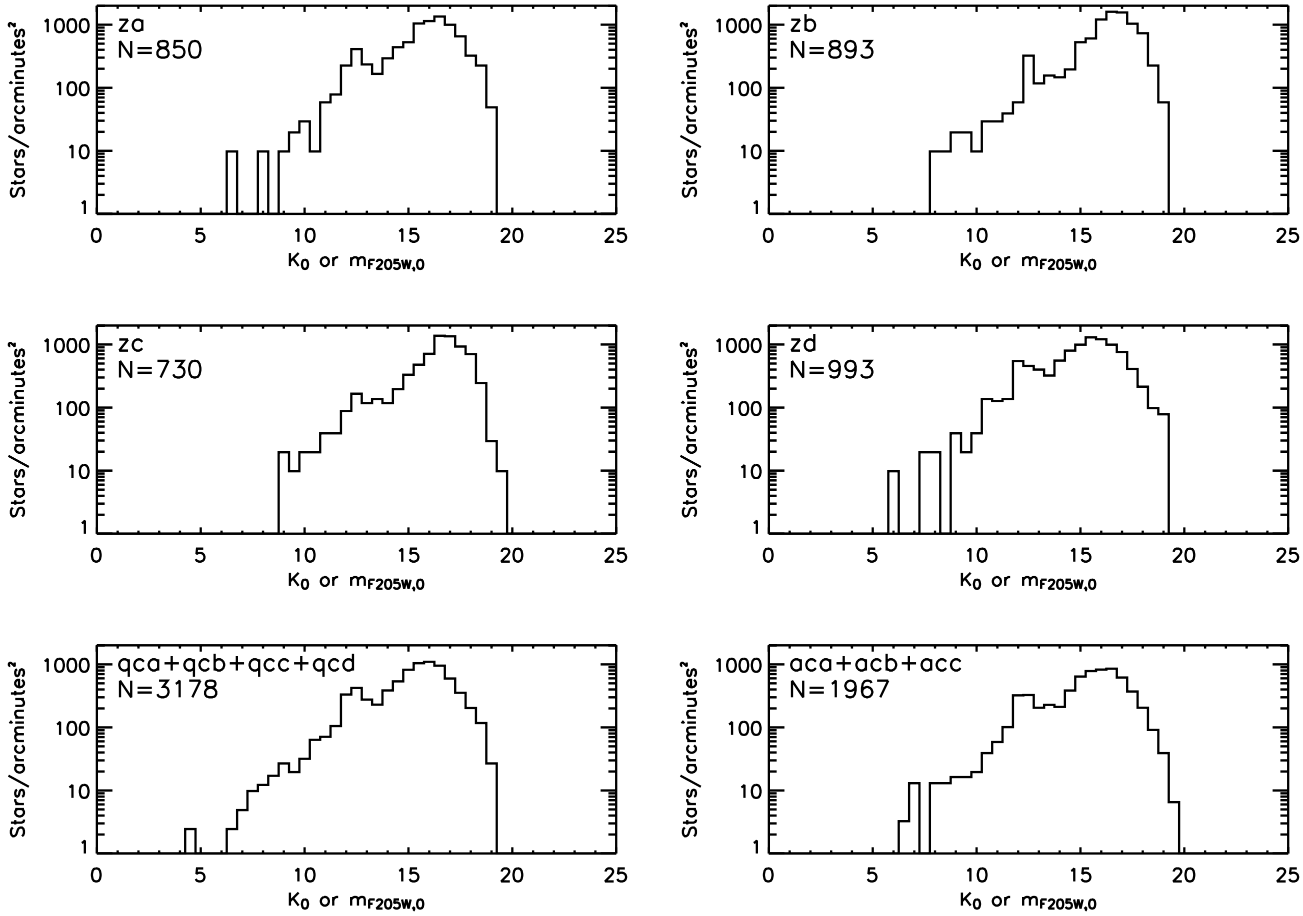

FIG. 4.—Dereddened LFs for individual NICMOS fields, as extracted from the CMDs in Fig. 3; the data have not been corrected for incompleteness. The red clump can generally be seen near $m_{\rm F205W} \approx 12.5$, although it is shifted toward brighter magnitudes for fields closer to the GC. Evidence of relatively young stars (hundreds of Myr old) in the main-sequence gap (e.g., Fig. 3) can be seen in the LF for the zd field.

"short-" ($\tau_{\rm exp} = 1$ s) and "long-" ($\tau_{\rm exp} = 30$ s) exposure images were used.

The NICMOS data include 12 fields obtained with the NIC2 camera (19."2 on a side) in the F110W ($\lambda_{\rm cen} = 1.10$ μm), F160W ($\lambda_{\rm cen} = 1.60$ μm), and F205W filters ($\lambda_{\rm cen} = 2.05$ μm). We selected these fields on the basis of a number of criteria: avoidance of crowded regions (thus excluding the centralmost region), avoidance of young star clusters, avoidance of regions of high extinction, and inclusion of fields ranging over a variety of Galactic latitudes and longitudes. Because extant near-IR maps of the Galactic nucleus, i.e., from the Two Micron All-Sky Survey (2MASS), show extensive regions of deep extinction just above and below the actual GC, our observations consisted mainly of a vertical strip of positions at a Galactic longitude offset, Δl, of 12′ from our Galaxy's central radio point source Sgr A* (our "*b*-strip"), as well as one field located along the true Galactic plane, at half the longitude offset of our vertical strip (our *l*/2 position). Observation of these undistinguished "background" fields in the nuclear cluster was obtained in concert with our observations of the young Arches and Quintuplet clusters. Those cluster observations also included four "off" positions surrounding each cluster. The exposure times were 255 s for each image.

We use aperture photometry with $d_{\rm aper} = 4."2$, or 6 pixels, for the Lick data set, with zero-point calibration set by photometry of several bright stars in the mosaic area from the

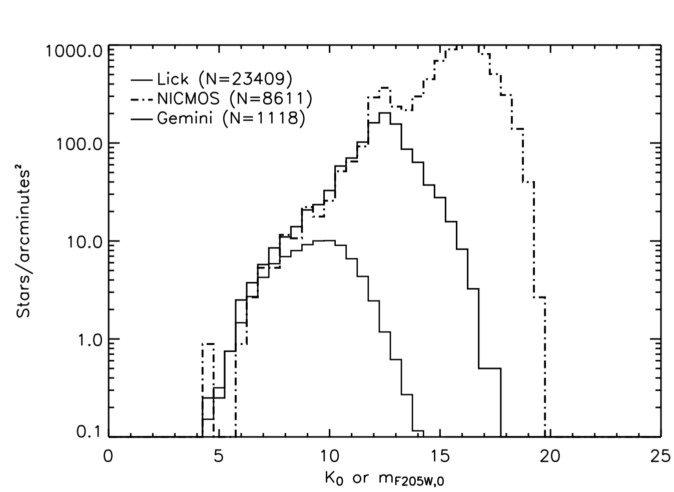

FIG. 5.—Dereddened LFs for the GC NICMOS (*dot-dashed line*), Lick (*light solid line*), and Gemini AO fields; the data have not been corrected for incompleteness. The three LFs match quite well over the magnitude ranges for which they are complete. The Lick data are already seriously incomplete at $K_0 \approx 9$, and the Gemini data begin to be incomplete at $K_0 \approx 12$, or roughly the magnitude of the red clump.

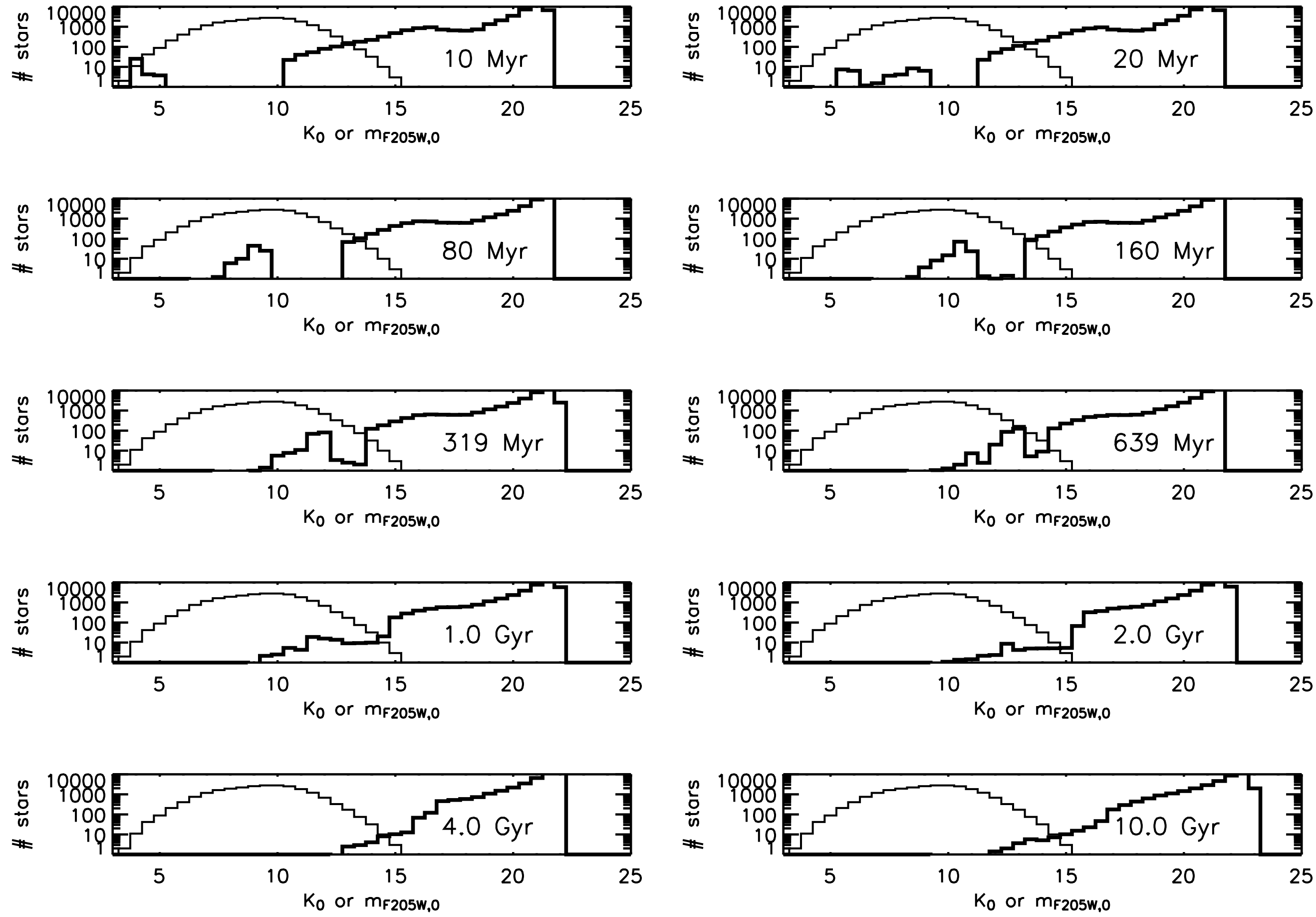

FIG. 6.—Theoretical (*heavy lines*) and observed (*light lines*) LF for the GC Lick field. The ages of the single starbursts assumed for the models are shown. We assume solar metallicity and the canonical mass-loss rates in the Geneva models. The starburst models used in making this figure are used in creating the summed LFs for more complex star formation histories in later figures. Note that we have not normalized the counts in this plot. The plots show that the observed counts at the brightest magnitudes cannot be reproduced by any single starburst. Note, also, that the counts at the bright end require the presence of some young stars.

literature. We used point-spread function–fitting photometry for both the *HST* NICMOS and Gemini AO data sets. Zero-point calibration for the *HST* NICMOS data was taken from MacKenty et al. (1997), with specific details relevant to our data set, including completeness corrections, discussed in

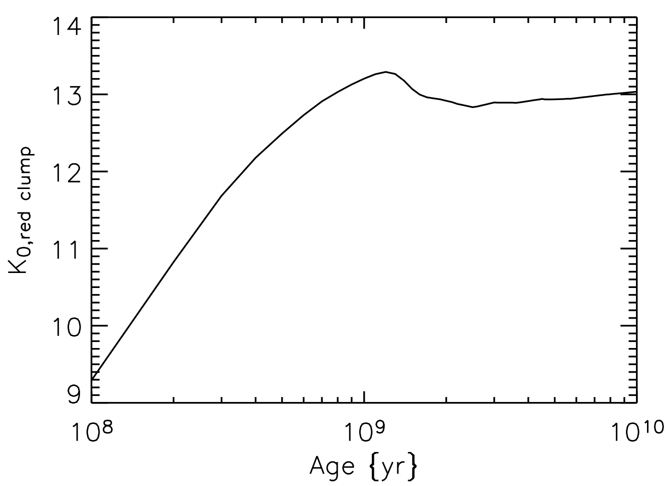

FIG. 7.—Dereddened K-band magnitude of red clump for a model starburst population in the GC as a function of age, adapted from Girardi et al. (2000), assuming solar metallicity.

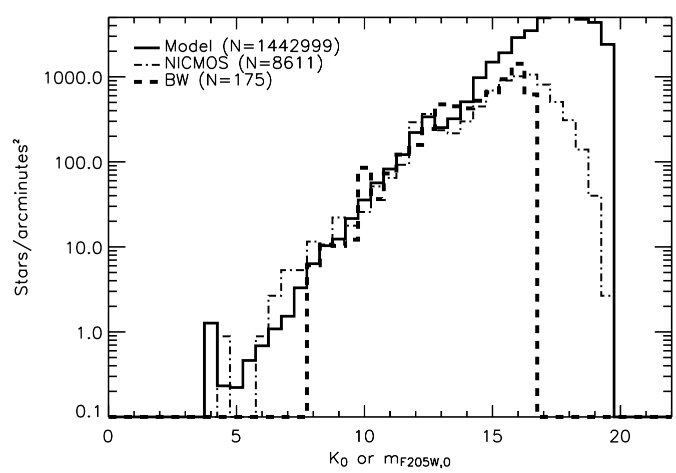

FIG. 8.—Theoretical (*solid line*) and observed LFs for Baade's window (*dashed line*) and the GC fields (*dot-dashed line*). The theoretical curve was produced using the Geneva models, assuming solar metallicity and a constant star formation rate of 0.07 $M_{\odot}$ yr^{-1} from 10 Gyr ago to the present. The Baade's window stars were arbitrarily scaled so that the counts roughly match the counts in the NICMOS data. Note the fainter red clump in the Baade's window data.

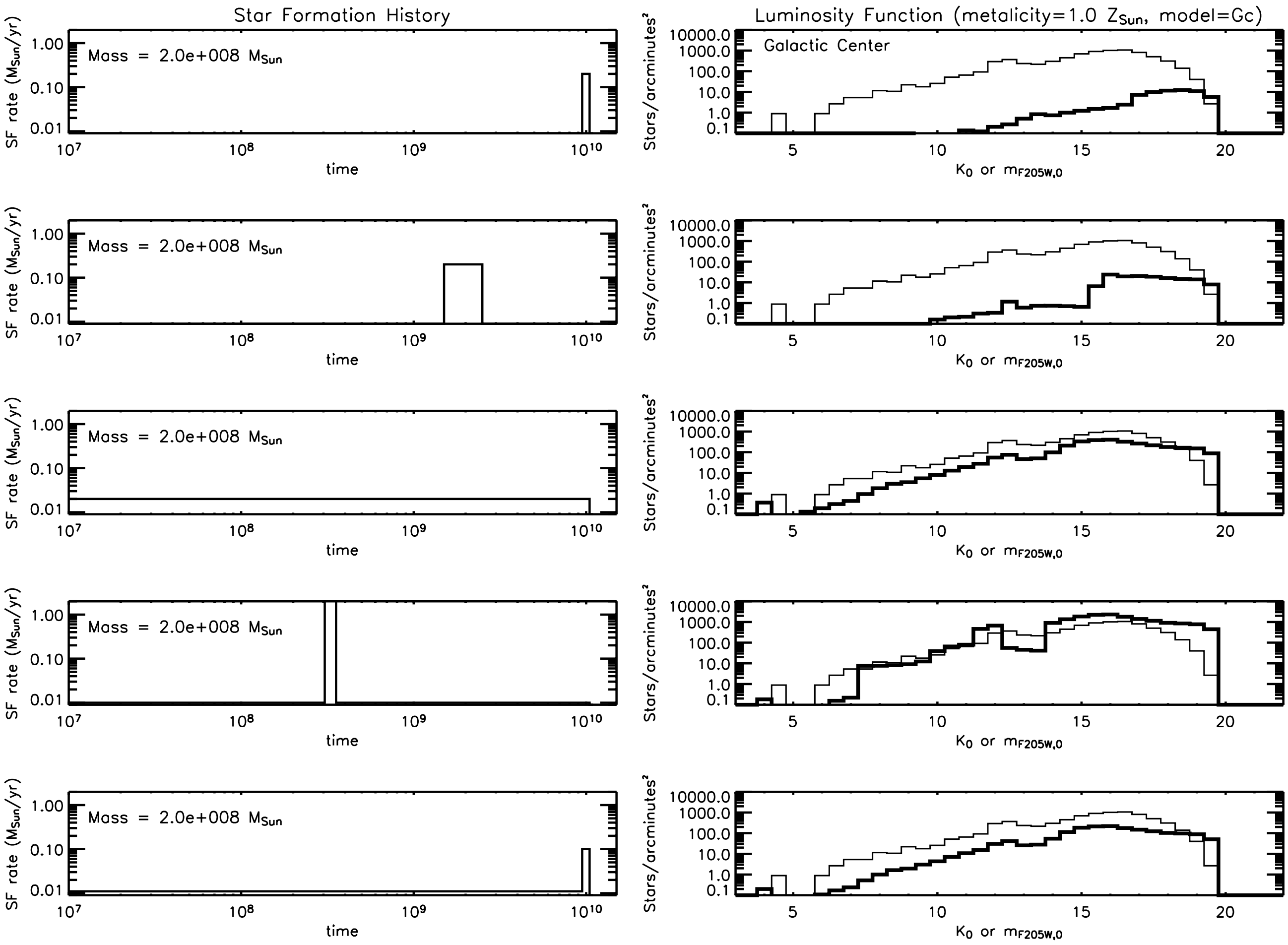

FIG. 9.—Model LFs (*heavy lines, right*) as a function of star formation scenario (*left*) for $Z = Z_{\odot}$ and the canonical mass-loss rates of the Geneva models, compared to the observed LF for the GC fields (*light lines, right*). The model counts have been multiplied by the completeness fraction of the observations. The models have been constrained to produce 2×10^8 $M_{\odot}$ over a circular area having $r < 30$ pc. Continuous star formation histories fit better than ancient bursts.

Figer et al. (1999a). The Gemini AO zero-point calibration was set by photometry of several stars in Blum, Sellgren, & DePoy (1996). The Gemini and Lick K' data were converted into K data using the observed $H-K'$ values and the relation of Wainscoat & Cowie (1992).

3. ANALYSIS AND RESULTS

3.1. *Color-Magnitude Diagrams*

Color-magnitude diagrams (CMDs) for the three data sets are shown in Figure 2. We can see that the NICMOS data continue down to about $m_{\rm F205W} = 21$ ($M_{\rm init} \sim 1.2$ $M_{\odot}$), roughly the magnitude for which the signal-to-noise ratio is $\sim$5. This is about 4 mag fainter than the Gemini AO data and about 1 mag fainter than the data in Genzel et al. (2003). The data are complete at the 50% level at $m_{\rm F205W} = 19.3$ ($M_{\rm init} \sim 2.2$ $M_{\odot}$), averaged over all fields. The Gemini AO data include objects just faint enough to distinguish the "red clump" near $K \sim 15.5$. The Lick data are already incomplete at $K \sim 12$, but they cover a much larger area than the other data sets, giving us more complete statistics at bright magnitudes.

CMDs for the individual NICMOS fields are shown in Figure 3. The trend in extinction for these fields is as expected, in that the fields closest to the GC suffer the greatest extinction, e.g., the zd field. Apparently, stars in the za, qc, and ac fields are commingled with ambient molecular material that serves to spread their locations in the diagram; the same effect is observed in the Lick data for this location. The red clump population is prominent in all of the fields, although the feature in the zc field is weak. Differential reddening is prominent in each field and broadens the clump distribution in color along the direction of reddening (to the lower right). The rise in the LF at the main-sequence turnoff point (e.g., at $m_{\rm F205W} \lesssim 19$ and $m_{\rm F160W} - m_{\rm F205W} \sim 1.6$ in the za field) is seen clearly in all fields, except for zd (closest to the GC), where confusion sets in at brighter magnitudes.

The presence of the clump and the main-sequence turnoff in the LF makes a prominent gap in the stellar CMD, an indication that much of the population must be older than a few Gyr. The relatively wide ($\sim$4 mag) gap between the clump and main-sequence turnoff seems consistent with a population older than 10 Gyr. As we proceeded with this interpretation, however, we tried to fit old globular cluster LFs to our GC data and noticed that the red clump was too bright to be consistent with a purely old stellar population. After considerable rechecking and verification of our photometry, this puzzle led us to proceed with the analysis we report in this paper.

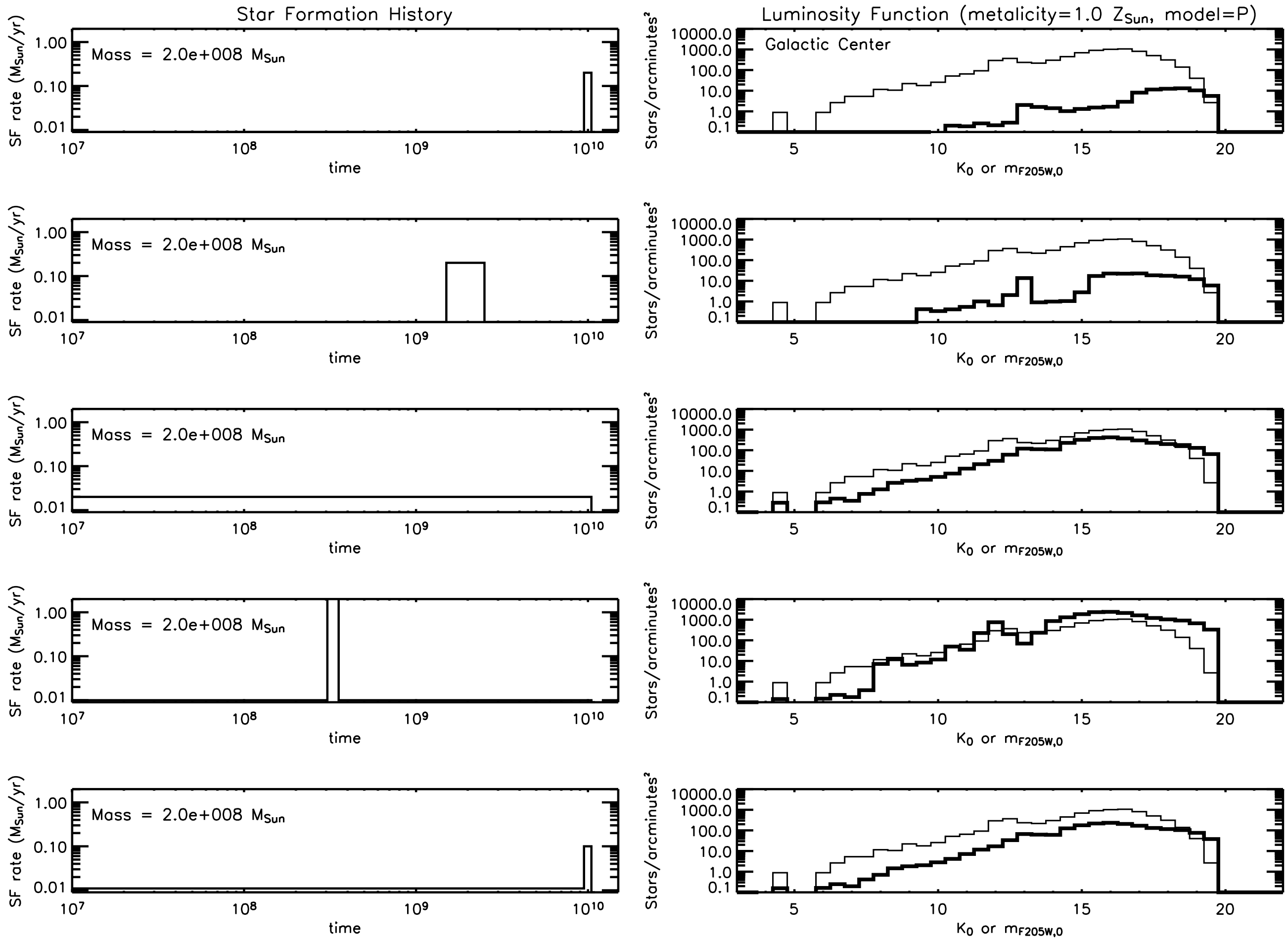

FIG. 10.—Same as Fig. 9, but using the Padova models

3.2. *Luminosity Functions*

In order to compare the observations to model predictions, we construct dereddened LFs by subtracting individual reddening values for each star based on its color in $H-K$ or $m_{\rm F160W}-m_{\rm F205W}$ and the assumption that each star has the intrinsic colors of a red giant. We estimate the intrinsic colors of a typical red giant by convolving the spectral energy distribution of a K4 III star from the Pickles (1998) library with the filter profiles, finding $(H-K)_0 = 0.11$ and $(m_{\rm F160W}-m_{\rm F205W})_0 = 0.24$. We deredden the photometry using the reddening law of Rieke, Rieke, & Paul (1989), i.e., $A_\lambda \propto \lambda^{-1.53}$. LFs for the individual NICMOS fields are shown in Figure 4.

Figure 5 shows the combined dereddened LFs for the NICMOS, Lick, and Gemini data. The "NICMOS" curve represents the sum of all the NICMOS fields, and it is scaled to account for the much larger area covered by the Lick survey. We find that $(m_{\rm F205W}-K)_0 < 0.05$ for red-clump stars, as measured by convolving the filter profiles with a spectral energy distribution of such stars; we thus make no explicit correction when comparing photometry in the two filters. The Lick data are confusion-limited for $K_0 > 9$, where the counts begin to roll over. The NICMOS LF appears to be a straight line, except for a bump at $K_0 = 12$, which represents the red clump. The two LFs appear to join for brighter magnitudes. The Gemini counts have been arbitrarily divided by 9 in order to scale them to match the NICMOS counts; the large difference in observed surface number density is expected, given that the Gemini fields are located much nearer to the GC than the NICMOS fields. The Gemini, Lick, and NICMOS data match very well, except for the weakness of the red clump in the Gemini data, a feature that is likely due to the incompleteness of the Gemini data.

3.3. *Star Formation Models*

We now infer the star formation history responsible for the observed populations by comparing their observed LFs to models built with both the Geneva and Padova isochrones. The Geneva models are described in Schaller et al. (1992), Schaerer et al. (1993a, 1993b), Charbonnel et al. (1993), and Meynet et al. (1994). They cover a grid of metallicities ($Z_\odot/20$, $Z_\odot/5$, $Z_\odot/2.5$, $Z_\odot$, and $2Z_\odot$), initial stellar masses (0.8–120 $M_\odot$), and two mass-loss–rate laws fo stars with $M_{\rm init} >$ 12 $M_\odot$ (the "canonical" and "enhanced" mass-loss–rate laws). We interpolate the evolutionary tracks and produce isochrones for a variety of masses and ages, extrapolating below 0.8 $M_\odot$. The Padova models were kindly provided by L. Girardi and are based on work described in Girardi et al. (2002). They cover the same metallicities as the Geneva models and initial stellar masses between 0.15 and 80 $M_\odot$. We do not use the Padova isochrones to model starbursts that are young enough to still include stars with $M_{\rm init} > 80$ $M_\odot$ (several Myr).

The model LFs for a given star formation history are produced by summing individual LFs for separate star formation

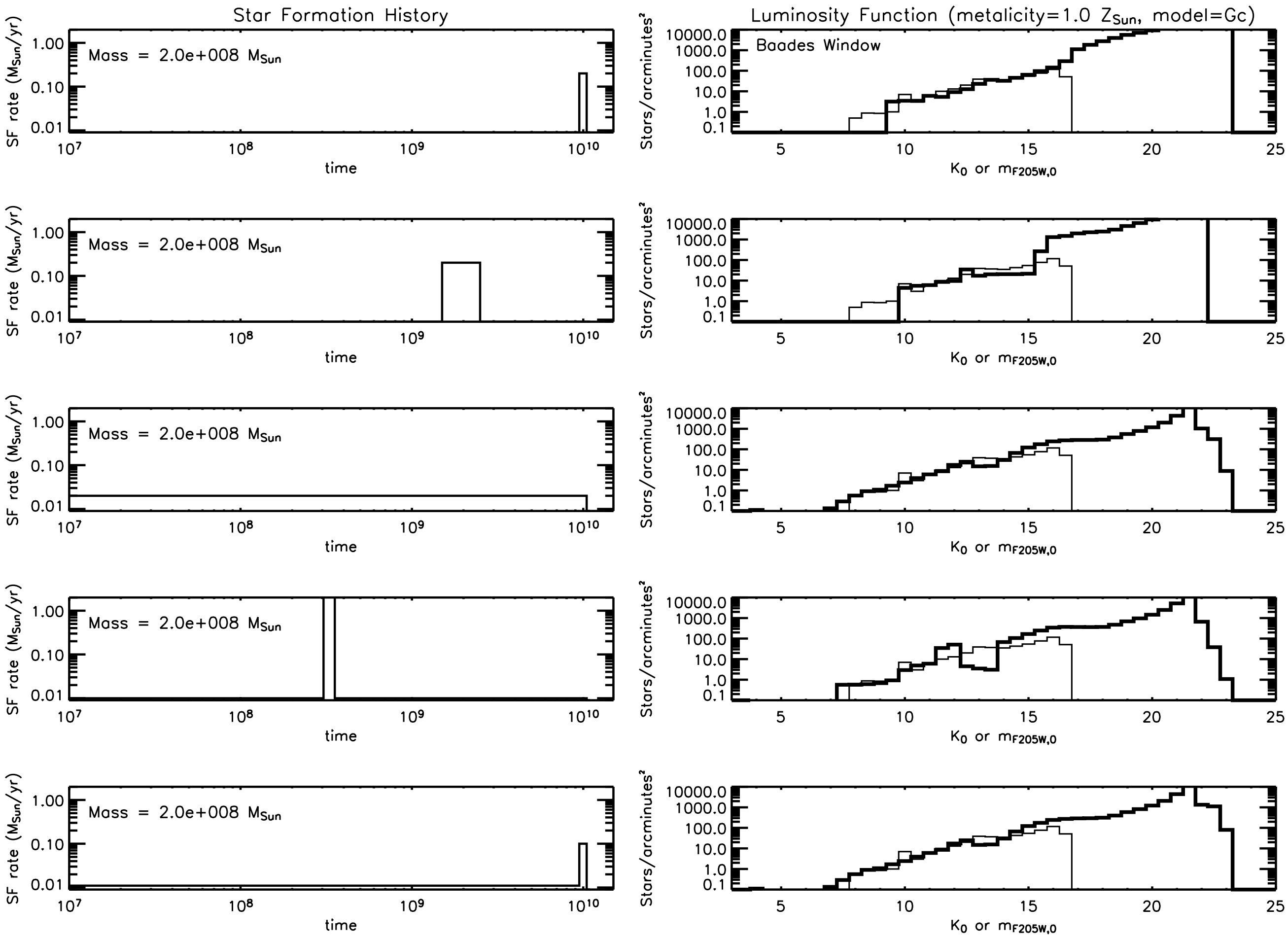

FIG. 11.—Same as Fig. 9, but for the Baade's window fields (*light lines, right*). The models have not been scaled for mass, but rather have been arbitrarily scaled along the vertical axis to match the observed counts in the $K = 11.0$ bin.

events, under the constraint that the total mass in stars formed is equal to 2×10^8 $M_\odot$, the mass inferred from velocity measurements in McGinn et al. (1989) within a projected radius of 30 pc of the GC. The individual events start at an age of 10^7 yr and are separated by 10^7 yr up to 10^9 yr, at which point they are spaced by 10^9 yr, up to $10^{10.1}$ yr. The number of stars formed in each event determines the normalization of the integral over a mass spectrum of stars given by a power law with index of -0.9, i.e., $dN/dm = m^\Gamma = m^{-0.9}$, as opposed to the Salpeter value of -1.35 (Salpeter 1955); this value is motivated by the measurements for the Arches cluster (Figer et al. 1999a; Yang et al. 2002; Stolte et al. 2003). The upper mass limit is 120 $M_\odot$, and the lower mass limit is 0.1 $M_\odot$. These masses are transformed to absolute magnitudes in the V band through the models. These are converted to absolute magnitudes in the band of interest, i.e., K, through a lookup table that relates color index to temperature (which comes from the models). The apparent magnitude in the band of interest is then simply the absolute magnitude plus the distance modulus (i.e., 14.52 for $d = 8$ kpc). We then sum the histogram to produce the LF and sum the individual LFs to produce the final LF for a given star formation history. The normalization to apparent surface density is fixed by dividing the model LFs by an "appropriate" area, 30π pc^2 throughout this paper. Note that this normalization produces a single "average" density for the whole area; i.e., no attempt was made to scale the densities with Galactocentric radius.

Figure 6 shows a subset of the starburst LFs that we use in constructing the summed LFs for various model star formation histories. In this figure, we illustrate a range of single starburst models, some of which are ultimately used in constructing our more complicated star formation models histories. We consider a range of ages, assuming the Geneva models with $Z = Z_\odot$ and canonical mass-loss rates. The Lick data are overplotted for comparison at the bright end ($K < 9$), where the data are reasonably complete. The LFs for young starbursts have a gap between the red supergiant stars and fainter stars that are still on the main sequence, a feature not seen in the Lick data. For older starbursts, the supergiants are gone and a horizontal branch/red clump forms (at $\sim$500 Myr). Note that the red-clump magnitude shifts to fainter, then brighter, over the time interval from 500 Myr to 2 Gyr. This effect is most clearly demonstrated in the plot adapted from Girardi et al. (2002) in Figure 7. This figure agrees well with observed data of red-clump stars for the ancient population of Baade's window, for which $m_{\rm RC} = 13.12$ (Alves 2000).

3.4. *Star Formation History*

The observations cannot be fitted by any single starburst population. However, there is promise in reproducing the observed features by constructing models for episodic, or continuous, star formation histories. We construct a model (Fig. 8) by assuming that the GC region continuously produced stars that evolved according to the Geneva models

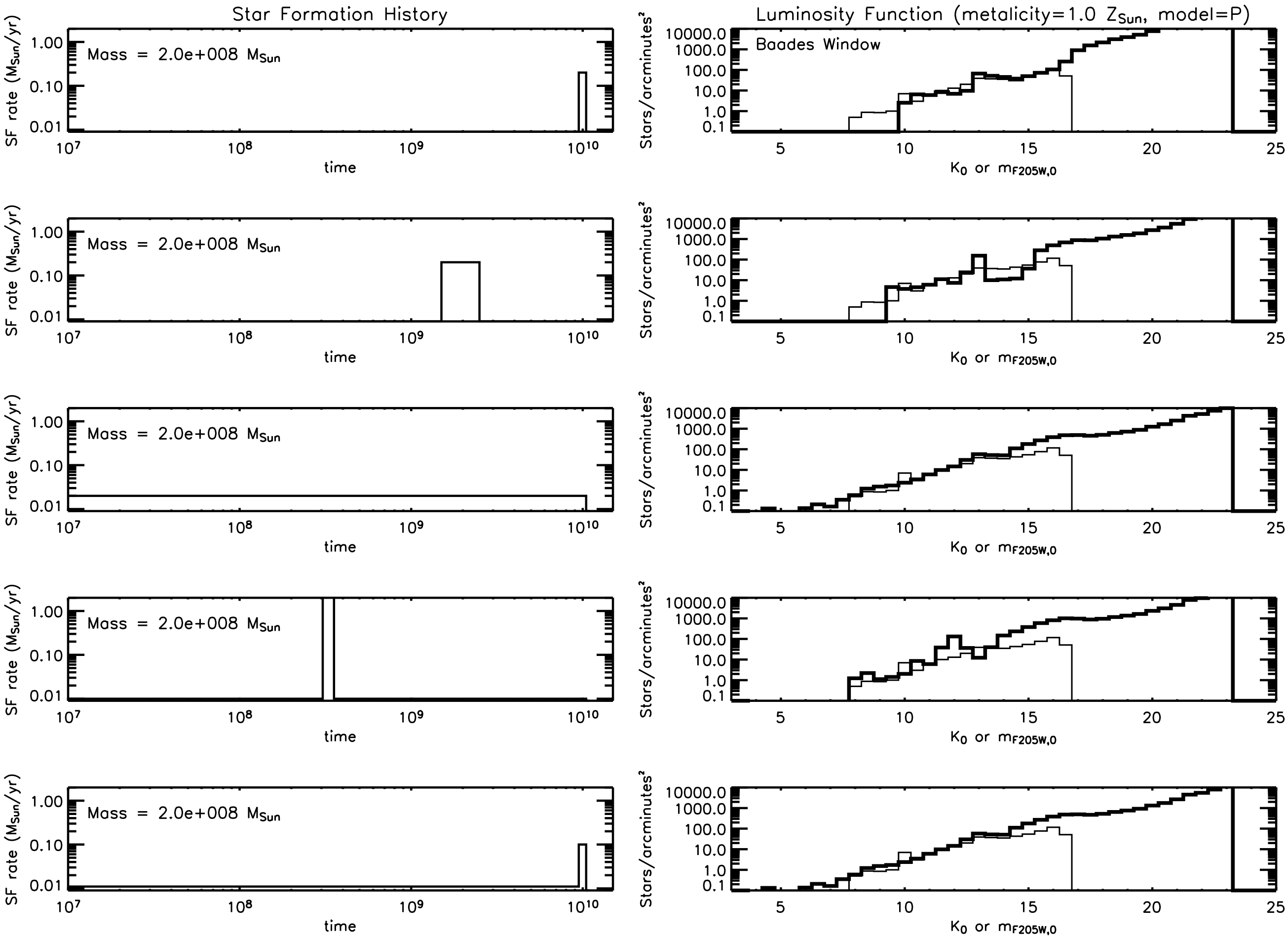

FIG. 12.—Same as Fig. 11, but using the Padova models

(Meynet et al. 1994). We assume that there was a burst every 10 Myr from 10 Gyr ago to the present, with an average rate of 0.07 $M_{\odot}$ yr^{-1}. We choose this rate so that the model curve fits the observed curve, but note that it is approximately 7 times the rate of the star formation that produced the three young clusters. The Tiede, Frogel, & Terndrup (1995) data of Baade's window stars were arbitrarily scaled so that the counts roughly match the counts in the scaled NICMOS data. The bright stars from the Lick data are well matched by our model. Indeed, the bright end of the LF can only be fitted by stars younger than $\approx$100 Myr. Our model also matches the red clump at $K_0 \sim 12$ very well. Most importantly, the model fits the absolute number of stars formed over the region modeled.

Figures 9 and 10 show alternate star formation scenarios, with the model counts modified by the observed completeness fractions from Figer et al. (1999a). The star formation histories are of three families: ancient bursts, continuous star formation, and bursts plus continuous star formation. In all cases, the histories produce 2×10^8 $M_{\odot}$ in stars within a radius of 30 pc.

There are five constraints provided by the models: (1) the counts in the bright end ($K_0 < 8$), (2) the slope at intermediate magnitudes ($10 < K_0 < 15$), (3) the brightness of the red clump, (4) the counts at the faint end ($K_0 > 15$), and (5) the absolute counts per unit area. The counts in the bright end are controlled by the extent of recent star formation. The slope is controlled by the presence of a red giant branch; note that any star formation history that includes some ancient stars will produce a red giant branch and thus an intermediate-magnitude slope that is a relatively constant function versus specifics within that history. The brightness of the red clump is related to the extent of star formation activity at intermediate age. The counts at the faint end are controlled by ancient star formation. The total number of counts in each bin is controlled by the strength and overall age of the star formation. Thus, we find that we can constrain the relative amounts of recent, intermediate, and ancient star formation activity through the use of these LFs, in addition to the absolute productivity of the star formation.

Figures 9 and 10 show that all five constraints are best fitted by the continuous star formation model. Indeed, the ancient bursts do not reproduce a bright end at all. The observed brightness of the red clump is too bright for intermediate-age bursts, whereas the continuous star formation scenario fits this constraint well. The counts at the faint end are overpredicted in the ancient-burst models, but they are reasonably well fitted by the continuous star formation model. Note that the data are much more than 50% incomplete for the faintest few bins. Most importantly, the absolute numbers of stars at intermediate magnitudes cannot be reproduced by the ancient-burst models. Indeed, the ancient-burst models fail badly at reproducing the number of stars seen, by 2 orders of magnitude in the brightest bins, even though the bursts assume a burst mass of 2×10^8 $M_{\odot}$.

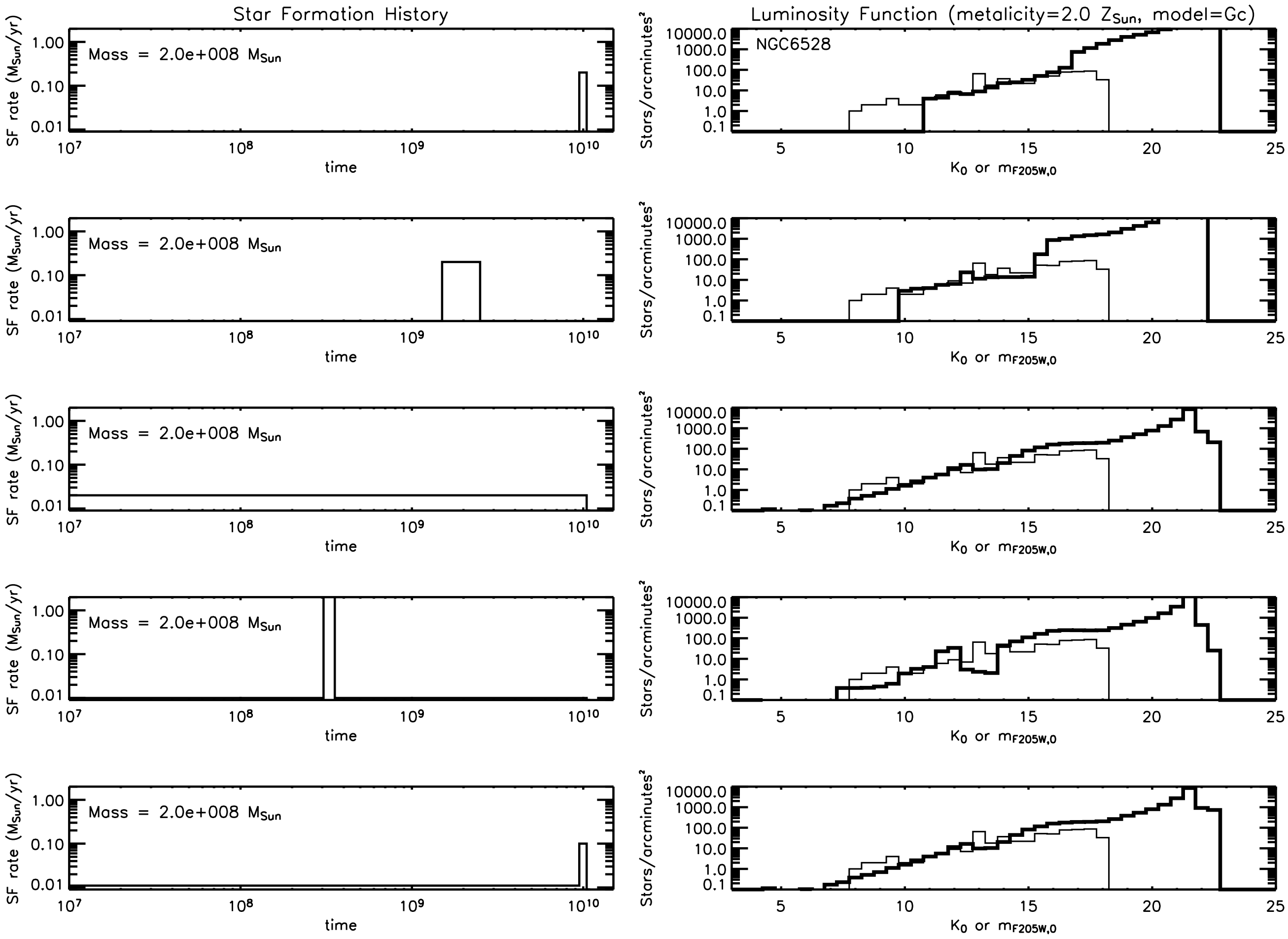

FIG. 13.—LFs (*heavy lines, right*) as a function of star formation scenario (*left*) for $Z = 2\ Z_\odot$ and the canonical mass-loss rates of the Geneva models, compared to the observed LF for the NGC 6528 field (*light lines, right*). The models have not been scaled for mass, but rather have been arbitrarily scaled along the vertical axis to match the observed counts in the $K = 11.0$ bin.

The qualitative analysis above begs the question of uniqueness. In order to determine the sensitivity of our technique, we attempt to model the old populations in Baade's window and in the Galactic globular cluster NGC 6528. Because we do not have reliable total mass constraints, unlike the situation for the GC, we scale the observed counts arbitrarily to achieve the best fit. Figures 11 and 12 show the results for Baade's window data. For Baade's window, the ancient-burst model provides the best fit, reproducing the faintness of the red clump and the counts at the faint end. Note, however, that the number of stars having $8 < K < 10$ is not reproduced by the ancient-burst models, because the models fail to faithfully model the upper tip of the asymptotic giant branch (AGB) LF. The AGB is the most poorly understood evolutionary phase, and therefore it will be most poorly fitted by any theoretical model. Further, the AGB luminosity has relatively low sensitivity to age at solar metallicity. Finally, the lifetimes are short, so the number counts of stars tend to be low. For these reasons we do not place most of the weight on the bright end of the AGB. The next-best fit is provided by the continuous star formation model, although the counts at the faint end and the brightness of the red clump are not well reproduced.

Figures 13 and 14 show the results for NGC 6528. We use models for metallicity twice that of the solar value, in accordance with the measured abundances in the NGC 6528 cluster stars (Carretta et al. 2001). Again, the figures show that the ancient-burst model provides the best fit. The observed red clump is more pronounced than that seen in the Geneva model, and it is very well fitted by the Padova model, as is a second bump 1 mag fainter ($K = 14.0$). As in the case of Baade's window, the next-best fit is given by the continuous star formation scenario. Just as before, this model for this scenario fails to match the observed faint end and the brightness of the red clump.

Next, we investigate the star formation history as a function of field location. Figures 15, 17, 19, and 21 show the completeness-corrected models overplotted on the individual observations in the z-fields for the Geneva models, and Figures 16, 18, 20, and 22 show the same for the Padova models. The LFs show that brighter stars are preferentially located closer to the GC and are absent for the zc field ($m_{\rm F205W} < 9$). Note that this is not a sampling effect, given that the fields are the same size. The brightness of the red clump is well fitted in all cases, although the observed clump for the zd field extends over several bins. The overall number of stars is also noticeably elevated for the zd field. We suggest that all of these effects are owed to more recent star formation closer to the GC. With greater areal sampling, we hope to constrain the star formation history as a function of position in the GC beyond the suggestive variations we already see in the z-fields.

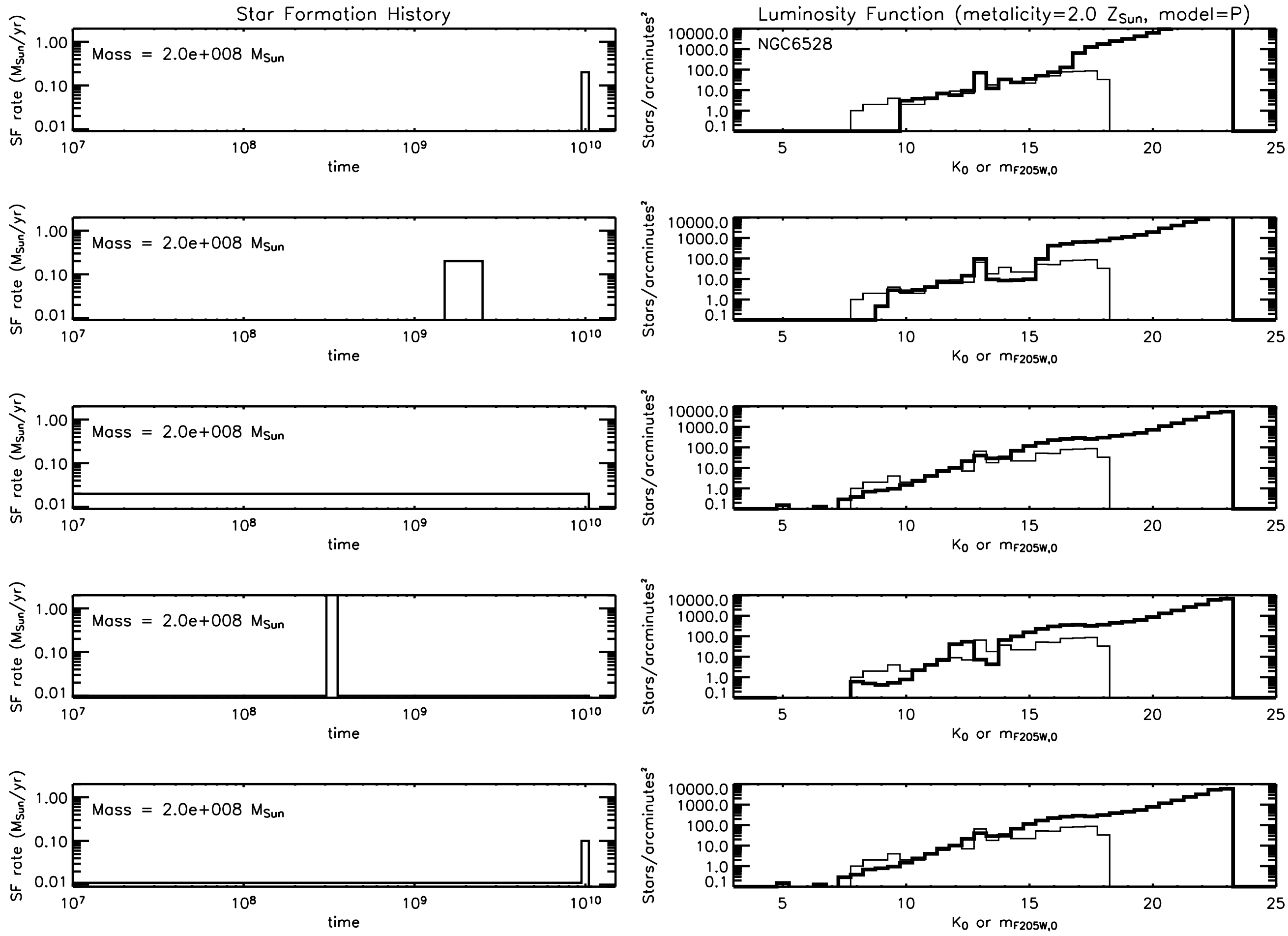

FIG. 14.—Same as Fig. 13, but using the Padova models

3.5. *Uniqueness*

We also ran models for a lower mass cutoff ($m_{\rm lower}$) of 1 $M_\odot$, instead of 0.1 $M_\odot$. That primarily resulted in a vertical shift upward of the LFs for $K_0 < 22$. While this elevated lower mass cutoff is consistent with the observations, we note that the absolute vertical scale for the models is more uncertain than the difference seen between the two cases of lower mass cutoffs. The results are also generally robust against variations in $m_{\rm upper}$, $\dot{M}$, Z, and Γ, within a factor of 2 in each parameter.

4. DISCUSSION

Although the presence of the red-clump population is consistent with a population older than 1 Gyr, our modeling of the observed LF points strongly in the direction of a continuous star formation history. The number counts and shape of the LF are inconsistent with a population dominated by an ancient burst or by a small number of bursts older than 1 Gyr. We favor a continuous star formation history with a rate of $\sim$0.02 $M_\odot$ yr^{-1}, or twice the rate inferred by the presence of the bright young clusters in the region. This rate appears to produce too few stars to match the observations, but it is bounded by the present enclosed mass of 2×10^8 $M_\odot$ within 30 pc of the GC. A more refined estimate of the rate will depend on careful normalization of the modeled surface number density. The young clusters currently observed were formed at an average star formation rate of 0.01 $M_\odot$ yr^{-1} over the past 5 Myr, in good agreement with the conclusions of this paper.

4.1. *Comparison to Other Work*

There is an abundant body of work noting the very young stellar population ($\tau_{\rm age} < 10$ Myr) in the central few arcminutes and additional studies noting intermediate-age populations on size scales observed in this paper. In particular, Narayanan et al. (1996), Haller (1992), and Blum et al. (1995) note an overabundance of bright stars in this region, compared to the number in Baade's window. Frogel et al. (1999) also note a dramatic increase in the number of bright stars compared to Baade's window. Our observations are consistent with these studies in showing an increase in the number of bright stars from the field farthest away from the GC (zc) to the closest (zd). Our results are consistent with previous work finding evidence for an intermediate-age stellar population in the GC. Sjouwerman et al. (1999) identified a population of OH/IR stars having high wind velocities, suggesting a starburst $\sim$1 Gyr ago. Our analysis rules out the possibility that the bulk of stars in the region formed in such a burst, although the analysis could accommodate a modest sized burst at $t =$ 1 Gyr, if accompanied by continuous star formation at other times.

Genzel et al. (2003) published a *K*-band LF for stars in the central parsec, obtained with the Very Large Telescope AO. Their Figure 9 shows the observations and a fit by an ancient–single-starburst model, noting the good agreement in the brightnesses of the red clump and the overall slope, after accounting for young stars at the bright end in the observations. It

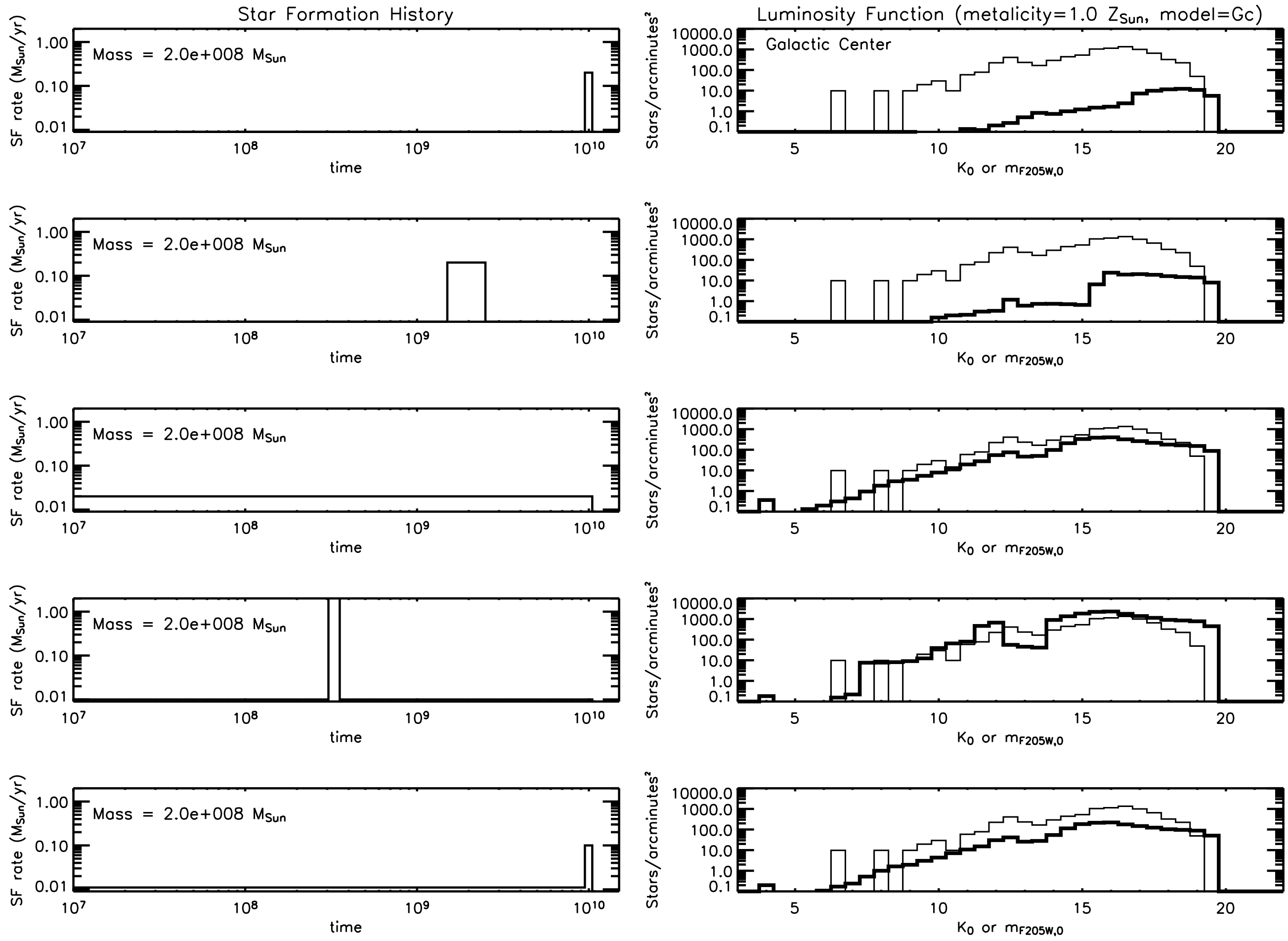

FIG. 15.—Same as Fig. 9, but for the GC za field (*light lines, right*). The model counts have been multiplied by the completeness fraction of the observations. The models have been constrained to produce 2×10^8 $M_\odot$ over a circular area having $r < 30$ pc. Continuous star formation histories fit better than ancient bursts.

is somewhat difficult to compare our results with those in Genzel et al. (2003), for several reasons. First, the Genzel et al. (2003) data are displayed in 1 mag wide bins, potentially smoothing the effect of a bright red clump. Second, the data are presented in the reddened reference frame, with a single extinction value being applied to the model. Our observations are first dereddened individually for each star and then compared to the models. This subtle difference can affect the detailed shape of the red clump when differential extinction is important. Finally, a detailed comparison would require that a single extinction law and common wavebands be used in both cases. Indeed, we infer a larger extinction for the central parsec than for our NICMOS fields, as shown in Figure 23, yet the extinction value in Genzel et al. (2003) ($A_K = 3.2$) is similar to the average extinction values for our NICMOS fields.

We do note, however, that our data produce a broad hump in the LF between $K = 10$ and 13 in the reddened frame (Fig. 8), similar to that seen in Figure 9 of Genzel et al. (2003). The fact that we see the feature in our data and in the Genzel et al. (2003) data leads us to believe that the feature is common to the central bulge, a result of ongoing star formation and not solely a product of the very recent star formation in the central parsec.

4.2. *Mass Budget*

The molecular clouds in the GC provide the material that feeds the star formation at a rate of a few hundredths of a solar mass per year (Morris 2001; Figer & Morris 2002). The star formation occurs within the CMZ, a disklike region of enhanced molecular density within a radius of $\sim$300 pc and having a thickness of $\sim$50 pc. The amount of molecular mass in the CMZ, about 5×10^7 $M_\odot$ (Morris & Serabyn 1996), would be consumed by star formation over relatively short timescales, $(2-4) \times 10^8$ yr. Therefore, there must be a source of replenishment. The ring of molecular material that circumscribes the CMZ at a Galactocentric distance of 150–180 pc is hypothesized to be material condensed into molecular form by shocks occurring along the innermost, non–self-intersecting x_1 orbit in the Galaxy's barred potential (Binney et al. 1991; Morris & Serabyn 1996). This feature is fed from the outside by gas migrating into the GC from the rest of the Galaxy. After shocking and condensing, the gas continues its inward migration and moves onto x_2 orbits inside the ring, where most of the molecular material in the CMZ resides (Regan & Teuben 2003). The inflow rate of material from the ring can be estimated by dividing the mass in the ring by the orbital period, 8×10^6 $M_\odot/2 \times 10^7$ yr $= 0.4$ $M_\odot$ yr^{-1}. This is an order of magnitude greater than the star formation rate estimated in this paper; however, the mass budget also includes a term for mass lost through a thermally driven wind (0.03–0.1 $M_\odot$ yr^{-1}). Clearly, all of the terms in the mass budget have errors that are large enough to permit the level of star formation claimed in this paper.

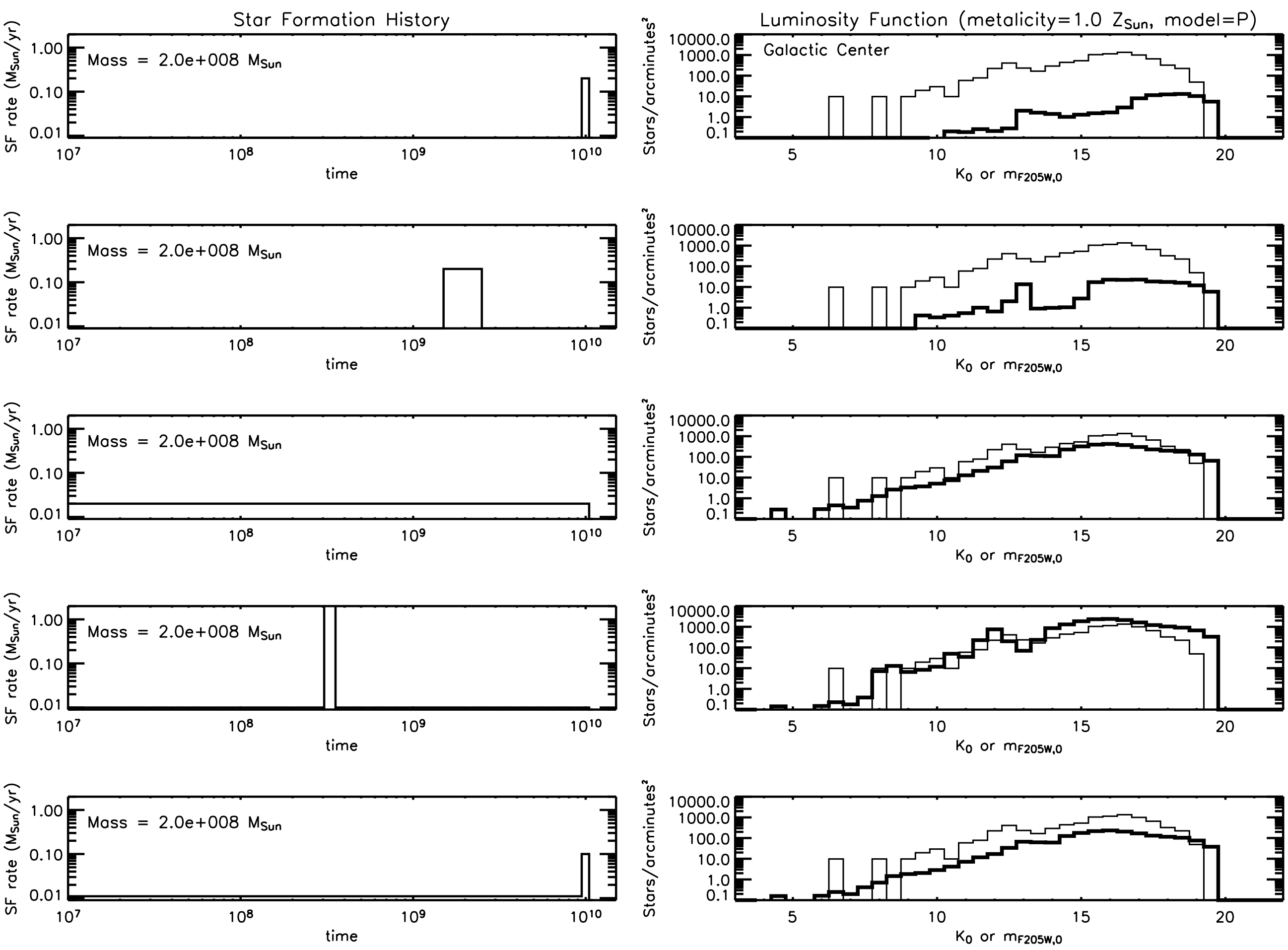

Fig. 16.—Same as Fig. 15, but using the Padova models

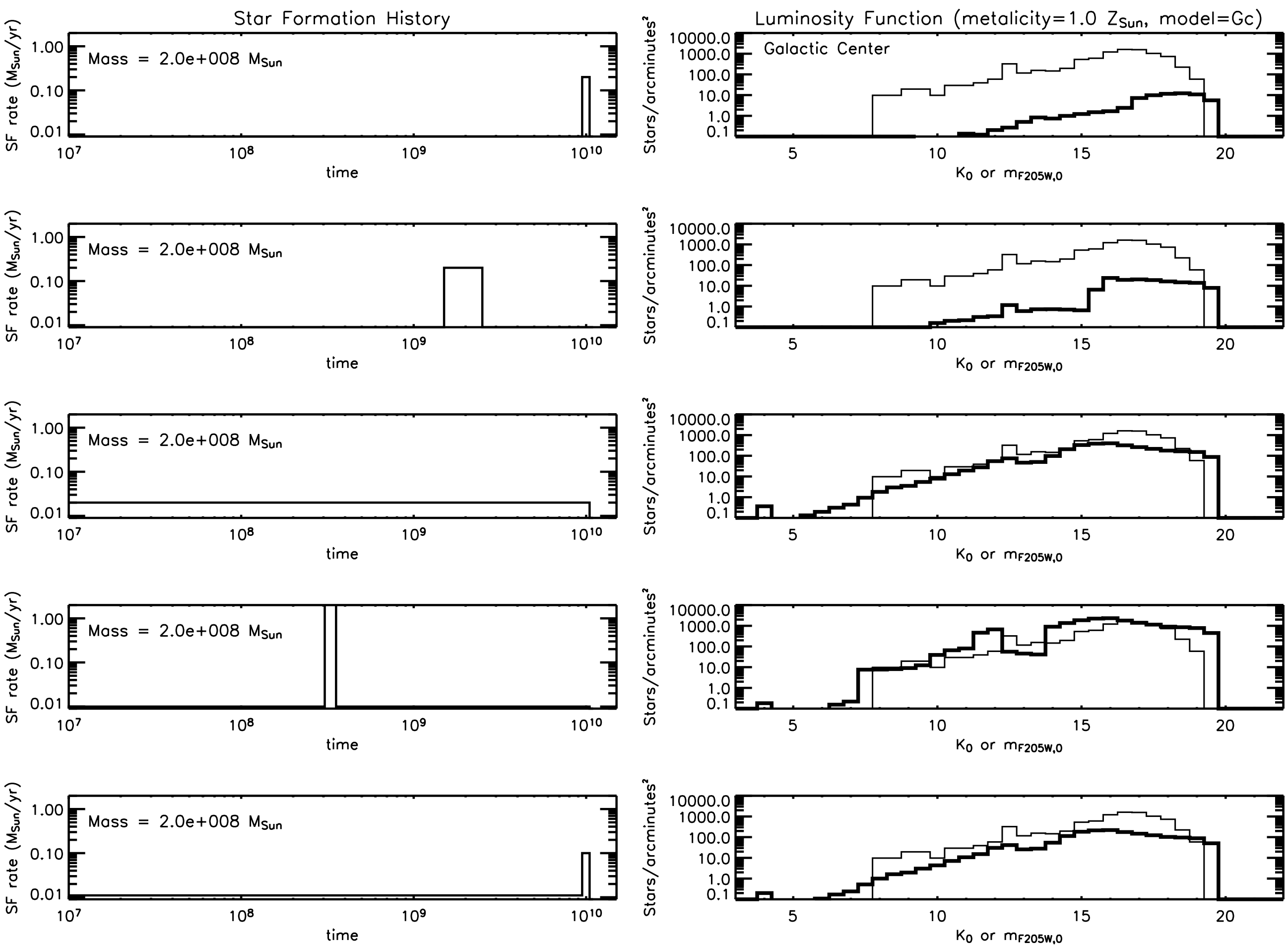

FIG. 17.—Same as Fig. 15, but for the GC zb field

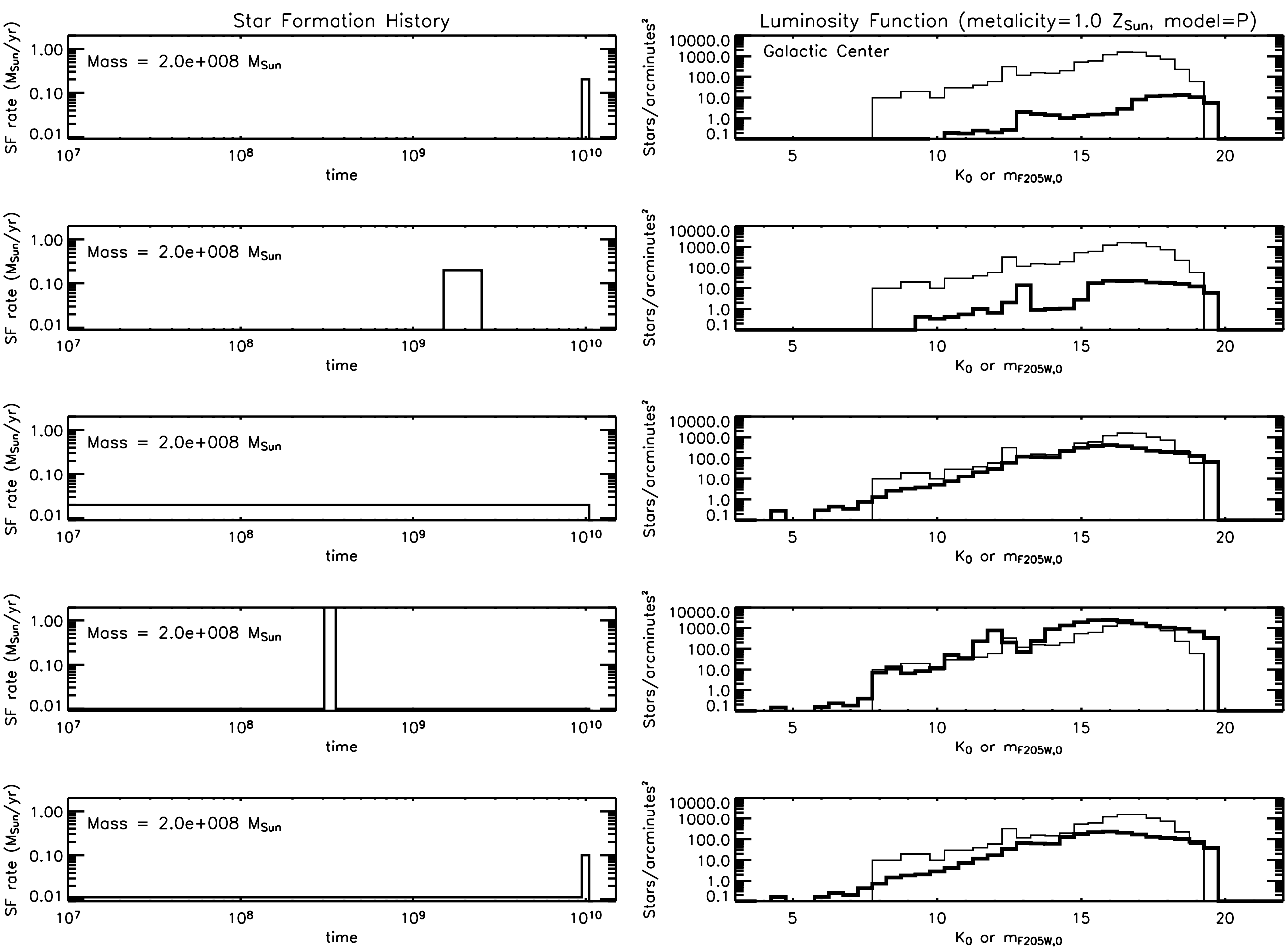

FIG. 18.—Same as Fig. 17, but using the Padova models

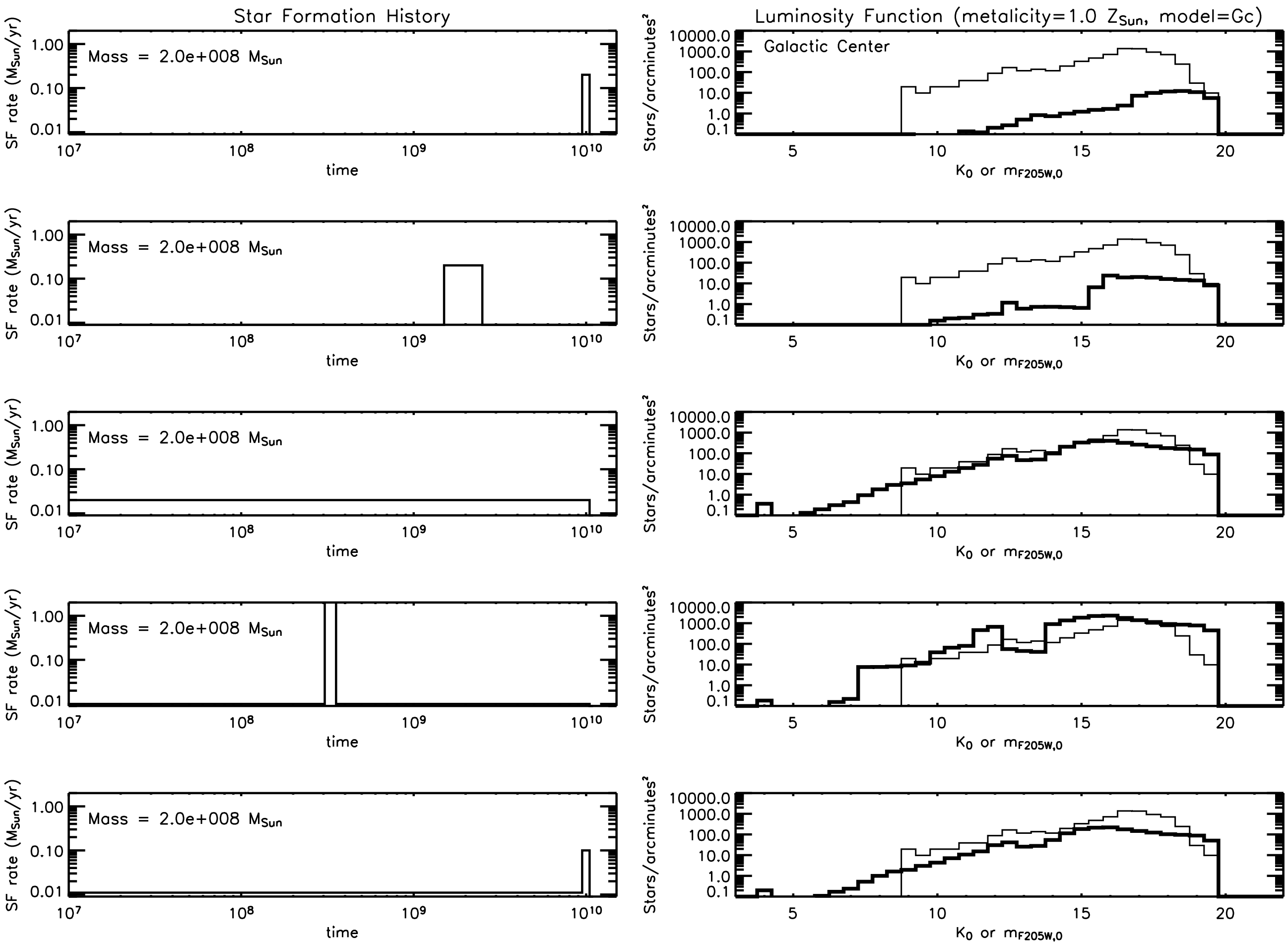

FIG. 19.—Same as Fig. 15, but for the GC zc field

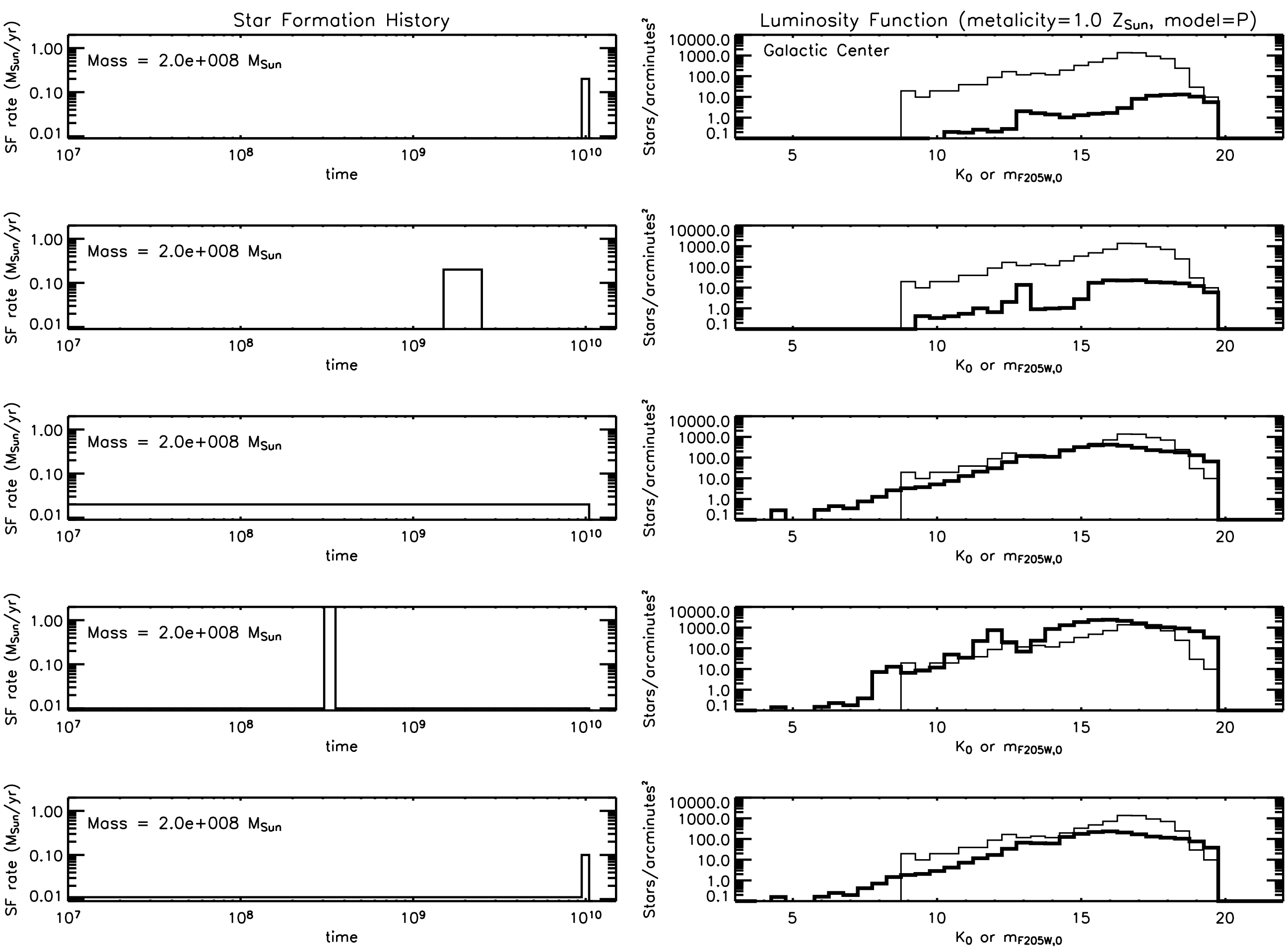

FIG. 20.—Same as Fig. 19, but using the Padova models

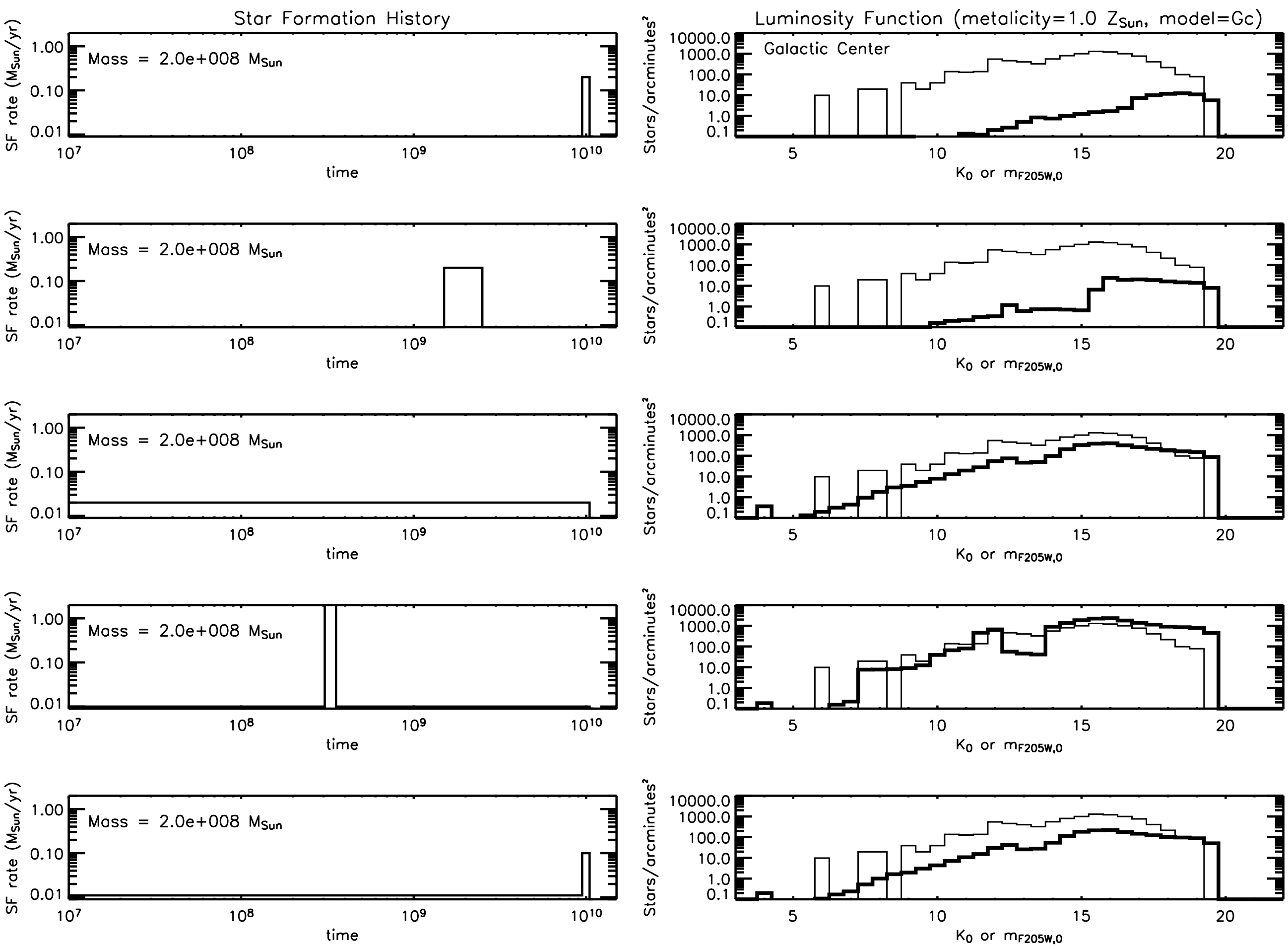

FIG. 21.—Same as Fig. 15, but for the GC zd field

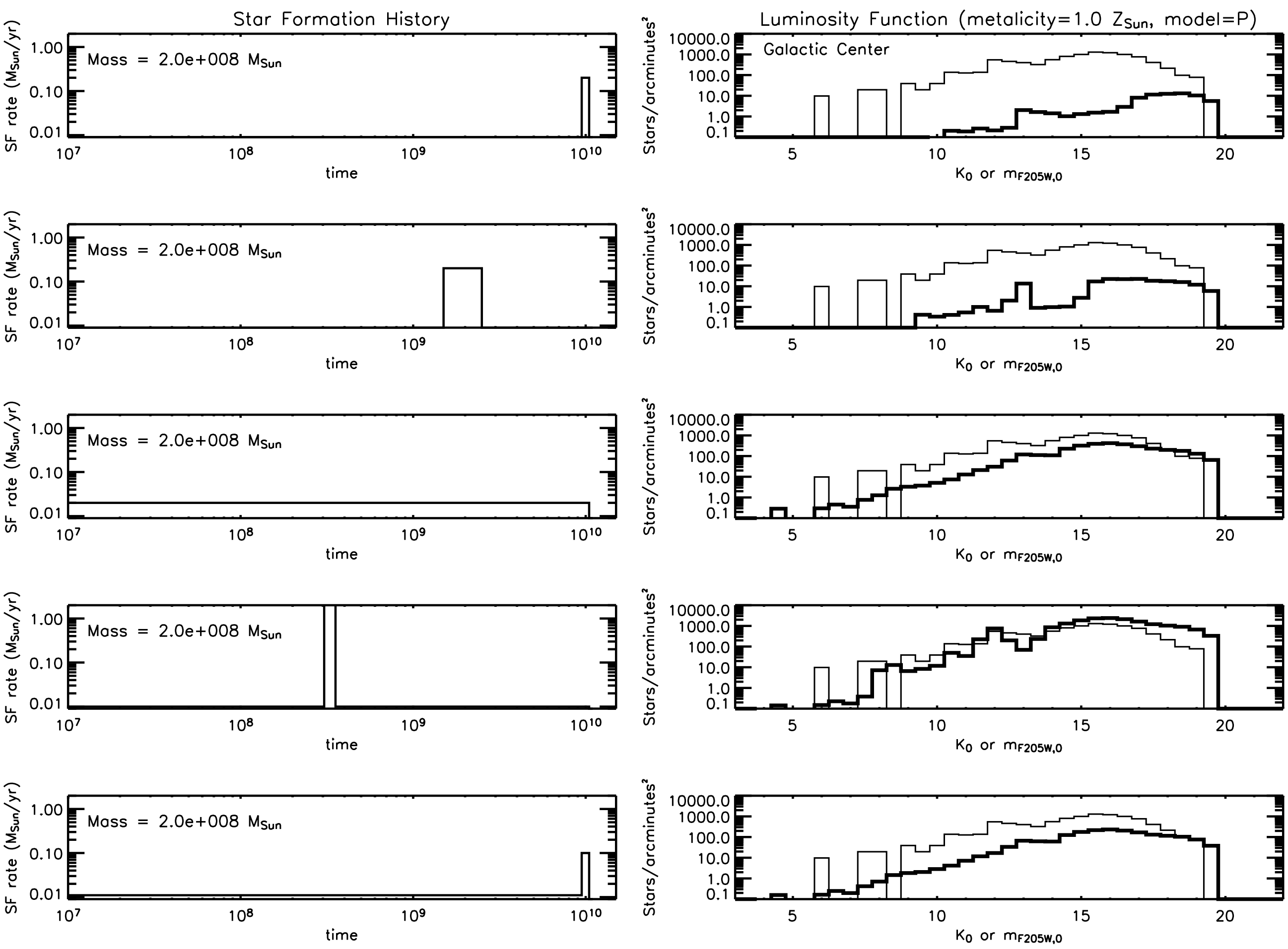

FIG. 22.—Same as Fig. 21, but using the Padova models

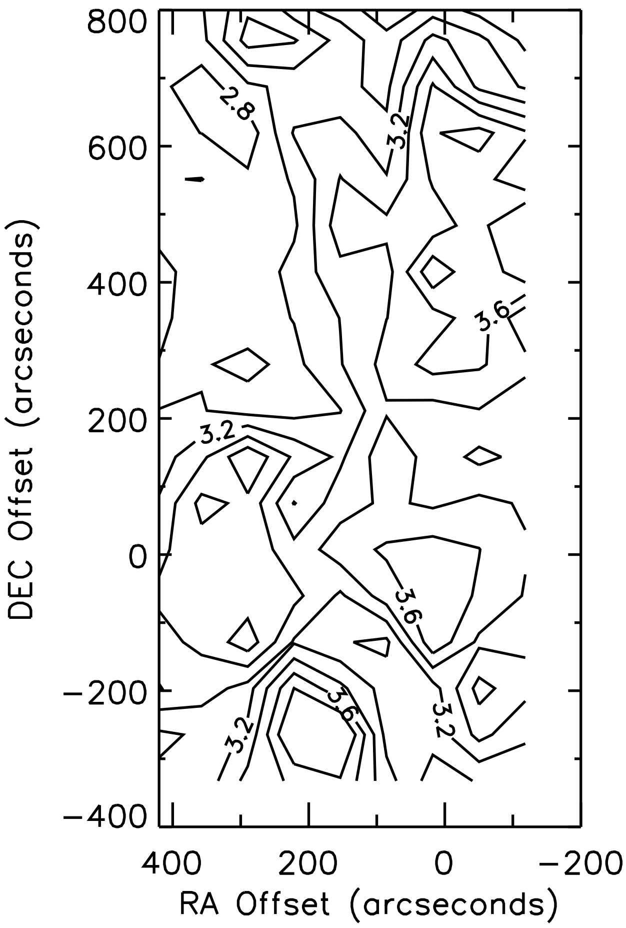

FIG. 23.—Extinction map (A_K), as inferred from the Lick data (Figer 1995). Sgr A* is located at (0, 0). The offsets are in arcseconds along right ascension and declination. See text for discussion.

4.3. *Relationship to Extragalactic Nuclear Populations*

Other than for the Milky Way, nuclei that harbor black holes and show no evidence of an AGN spectrum have stellar populations consistent with formation in an ancient burst (Magorrian et al. 1998). One must emphasize that black holes are more difficult to detect in galaxies with active star formation, so the kinematic sample is biased. Within the Local Group, the nuclei of M31 and M32 can be so characterized; while M32 may contain some fraction of few Gyr old stars, there is no evidence of recent star formation in the M32 nucleus. The unusual star formation history in the GC may be related to bar-induced feeding of gas into the central region and subsequent star formation (Regan & Teuben 2003).

Our demonstration that the star formation history of the nuclear population is continuous has additional implications and raises several questions. Has the black hole grown in mass along with the stellar population, or was most of the mass of the black hole in place, perhaps within a Gyr of the Galaxy's formation? Further, how can a galaxy with a bulge population well demonstrated to be as old as the oldest globular clusters (Ortolani et al. 1995; Kuijken & Rich 2002; Zoccali et al. 2003) have formed at early times without simultaneously forming the bulk of the stars currently seen in the nuclear population?

We thank Leo Girardi for graciously providing the Padova model isochrone files. We acknowledge very useful discussions with Mike Regan, Paco Najarro, Bob Blum, Laurant Sjouwerman, and Jay Frogel. We also thank the Gemini North Science Verification Team for obtaining the GC data used in this paper. Support for this work was provided by NASA through grants GO-07364.01-96A and AR-08751.02-A from the Space Telescope Science Institute, which is operated by AURA, Inc., under NASA contract NAS5-26555. Mark Morris is supported by NSF through AST 99-88397. Work by S. S. K. was supported by the Astrophysical Research Center for the Structure and Evolution of the Cosmos (ARCSEC) of the Korea Science and Engineering Foundation through the Science Research Center program.

REFERENCES

Alves, D. R. 2000, ApJ, 539, 732
Binney, J., Gerhard, O. E., Stark, A. A., Bally, J., & Uchida, K. I. 1991, MNRAS, 252, 210
Blum, R. D., DePoy, D. L., & Sellgren, K. 1995, ApJ, 441, 603
Blum, R. D., Sellgren, K., & DePoy, D. L. 1996, ApJ, 470, 864
Carretta, E., Cohen, J. G., Gratton, R. G., & Behr, B. B. 2001, AJ, 122, 1469
Catchpole, R. M., Whitelock, P. A., & Glass, I. S. 1990, MNRAS, 247, 479
Charbonnel, C., Meynet, G., Maeder, A., Schaller, G., & Schaerer, D. 1993, A&AS, 101, 415
Cotera, A. S. 1995, Ph.D. thesis, Stanford Univ.
Cotera, A. S., Erickson, E. F., Allen, D. A., Colgan, S. W. J., Simpson, J. P., & Burton, M. G. 1994, in The Nuclei of Normal Galaxies: Lessons from the Galactic Center, ed. R. Genzel & A. I. Harris (NATO ASI Ser. C, 445; Dordrecht: Kluwer), 217
Cotera, A. S., Erickson, E. F., Colgan, S. W. J., Simpson, J. P., Allen, D. A., & Burton, M. G. 1996, ApJ, 461, 750
Cox, P., & Laureijs, R. 1989, in IAU Symp. 136, The Center of the Galaxy, ed. M. Morris (Dordrecht: Kluwer), 121
Figer, D. F. 1995, Ph.D. thesis, UCLA
Figer, D. F., Kim, S. S., Morris, M., Serabyn, E., Rich, R. M., & McLean, I. S. 1999a, ApJ, 525, 750
Figer, D. F., McLean, I. S., & Morris, M. 1995, ApJ, 447, L29
———. 1999b, ApJ, 514, 202
Figer, D. F., & Morris, M. 2002, in ASP Conf. Ser. 285, Modes of Star Formation and the Origin of Field Populations, ed. E. K. Grebel & W. Brandner (San Francisco: ASP), 381
Figer, D. F., et al. 2002, ApJ, 521, 258
Frogel, J. A., Tiede, G. P., & Kuchinski, L. E. 1999, AJ, 117, 2296
Geballe, T. R., Genzel, R., Krabbe, A., Krenz, T., & Lutz, D. 1994, in Infrared Astronomy with Arrays: The Next Generation, ed. I. S. McLean (Dordrecht: Kluwer), 73
Genzel, R., Thatte, N., Krabbe, A., Kroker, H., & Tacconi-Garman, L. E. 1996, ApJ, 472, 153
Genzel, R., et al. 2003, ApJ, 594, 812
Gerhard, O. 2001, ApJ, 546, L39
Girardi, L., Bertelli, G., Bressan, A., Chiosi, C., Groenewegen, M. A. T., Marigo, P., Salasnich, B., & Weiss, A. 2002, A&A, 391, 195
Girardi, L., Bressan, A., Bertelli, G., & Chiosi, C. 2000, A&AS, 141, 371
Glass, I. S., Moneti, A., & Moorwood, A. F. M. 1990, MNRAS, 242, 55P
Haller, J. W. 1992, Ph.D. thesis, Univ. Arizona
Haller, J. W., & Rieke, M. J. 1989, in IAU Symp. 136, The Center of the Galaxy, ed. M. Morris (Dordrecht: Kluwer), 487
Hiromoto, N., Maihara, T., Mizutani, K., Takami, H., Shibai, H., & Okuda, H. 1984, A&A, 139, 309
Kim, S. S., Figer, D. F., Lee, H. M., & Morris, M. 2000, ApJ, 545, 301
Kim, S. S., & Morris, M. 2003, ApJ, 597, 312
Kim, S. S., Morris, M., & Figer, D. F. 2003, in The Central 300 Parsecs of the Milky Way, ed. A. Cotera, H. Falcke, T. R. Geballe, & S. Markoff (Astron. Nachr. Suppl., Vol. 324, S1), in press
Kim, S. S., Morris, M., & Lee, H. M. 1999, ApJ, 525, 228
Krabbe, A., et al. 1995, ApJ, 447, L95
Kuijken, K., & Rich, R. M. 2002, AJ, 124, 2054

Launhardt, R., Zylka, R., & Mezger, P. G. 2002, A&A, 384, 112
Lebofsky, M. J., & Rieke, G. H. 1987, in AIP Conf. Proc. 155, The Galactic Center, ed. D. C. Backer (New York: AIP), 79
MacKenty, J. W., et al. 1997, NICMOS Instrument Handbook, version 2.0 (Baltimore: STScI)
Magorrian, J., et al. 1998, AJ, 115, 2285
McGinn, M. T., Sellgren, K., Becklin, E. E., & Hall, D. N. B. 1989, ApJ, 338, 824
Meynet, G., Maeder, A., Schaller, G., Schaerer, D., & Charbonnel, C. 1994, A&AS, 103, 97
Moneti, A., Glass, I., & Moorwood, A. 1992, MNRAS, 258, 705
———. 1994, MNRAS, 268, 194
Morris, M. 2001, in Starburst Galaxies: Near and Far, ed. L. Tacconi & D. Lutz (Heidelberg: Springer), 53
Morris, M., & Serabyn, E. 1996, ARA&A, 34, 645
Nagata, T., Woodward, C. E., Shure, M., & Kobayashi, N. 1995, AJ, 109, 1676
Nagata, T., Woodward, C. E., Shure, M., Pipher, J. L., & Okuda, H. 1990, ApJ, 351, 83
Najarro, F., Krabbe, A., Genzel, R., Lutz, D., Kudritzki, R. P., & Hillier, D. J. 1997, A&A, 325, 700
Narayanan, V. K., Gould, A., & DePoy, D. L. 1996, ApJ, 472, 183
Okuda, H., et al. 1990, ApJ, 351, 89
Ortolani, S., Renzini, A., Gilmozzi, R., Marconi, G., Barbuy, B., Bica, E., & Rich, R. M. 1995, Nature, 377, 701
Pickles, A. J. 1998, PASP, 110, 863
Portegies Zwart, S. F., Makino, J., McMillan, S. L. W., & Hut, P. 2001, ApJ, 546, L101
Regan, M. W., & Teuben, P. 2003, ApJ, 582, 723
Rieke, G. H., Rieke, M. J., & Paul, A. E. 1989, ApJ, 336, 752
Rieke, M. J. 1987, in Nearly Normal Galaxies: From the Planck Time to the Present, ed. S. M. Faber (New York: Springer), 90
Rieke, M. J. 1993, in AIP Conf. Proc. 278, Back to the Galaxy, ed. S. S. Holt & F. Verter (New York: AIP), 37
Salpeter, E. E. 1955, ApJ, 121, 161
Schaerer, D., Charbonnel, C., Meynet, G., Maeder, A., & Schaller, G. 1993a, A&AS, 102, 339
Schaerer, D., Meynet, G., Maeder, A., & Schaller, G. 1993b, A&AS, 98, 523
Schaller, G., Schaerer, D., Meynet, G., & Maeder, A. 1992, A&AS, 96, 269
Serabyn, E., & Morris, M. 1996, Nature, 382, 602
Serabyn, E., Shupe, D., & Figer, D. F. 1998, Nature, 394, 448
Sjouwerman, L. O., Habing, H. J., Lindqvist, M., van Langevelde, H. J., & Winnberg, A. 1999, in ASP Conf. Ser. 186, The Central Parsecs of the Galaxy, ed. H. Falcke, A. Cotera, W. J. Duschl, F. Melia, & M. J. Rieke (San Francisco: ASP), 379
Stolte, A., Brandner, W., Grebel, E. K., Figer, D. F., Eisenhauer, F., Lenzen, R., & Harayama, Y. 2003, Messenger, 111, 9
Tiede, G. P., Frogel, J. A., & Terndrup, D. M. 1995, AJ, 110, 2788
Wainscoat, R. J., & Cowie, L. L. 1992, AJ, 103, 332
Yang, Y., Park, H. S., Lee, M. G., & Lee, S. 2002, J. Korean Astron. Soc., 35, 131
Zoccali, M., et al. 2003, A&A, 399, 931